Physics – Uspekhi **40** (6) 581 – 597 (1997)

REVIEWS OF TOPICAL PROBLEMS PACS numbers: 61.43.Dq, **75.10.–b**, 75.50.Kj

Magnetic properties of amorphous rare-earth – 3d-transition-metal alloys

A S Andreenko, S A Nikitin

Contents

Abstract. Work on the magnetic properties of amorphous rare-earth – 3d-transition-metal alloys is reviewed using current theoretical models to account for the experimental data available. The exchange interaction and random magnetic anisotropy are shown to dominate the magnetization and magnetization reversal processes. Some new phenomena related to the effect of induced magnetic anisotropy on magnetization processes are considered. The results on the magnetoelastic properties of rare-earth alloys are systematized. The dependence of the exchange integrals on the interatomic separation is determined. It is shown that pressure significantly affects the magnetic structure and phase transitions in these magnetic materials.

1. Introduction

The history of investigations of amorphous magnetic materials is relatively short. Before 1960, among scientists engaged in magnetism it was widely believed that magnetic ordering can occur only in crystalline materials. The possibility for magnetic ordering in non-crystalline metallic compounds was first substantiated theoretically by Gubanov in 1960 [1]. The next step in the study of amorphous magnets was a result of advances in the production of amorphous magnetic alloys based on the Fe-group magnetic metals with non-magnetic dopants such as silicon or boron playing the role of stabilizers of an amorphous phase.

In 1973, first reports on the production of amorphous alloys of rare-earth (RE) and 3d transition-metals (TM) (RE – TM alloys) appeared [2, 3]. Thereafter many investigators concentrated their attention on the study of this class of magnetic compounds. Interest in the research of these objects was stimulated by the fact that the absence of chemical, crystallographic and topological order in these alloys results in fluctuations of fundamental interactions determining the character of magnetic ordering in amorphous magnets.

Already the first investigations have shown that amorphous RE-TM alloys exhibit a number of unique properties. Magnetic bubbles [2], giant coercivity at low temperatures [4], magnetic angstrom-sized microdomains [5], an anomalous relationship between the magnetic-ordering temperature and the spin magnitude of rare-earth ions [5, 6] have all been found in these alloys.

The structural features of amorphous alloys called for development of new theoretical concepts that take into account the metastable character of their magnetic state and the fluctuations of the basic energy parameters determining the magnetic state of ions. This required a knowledge of the magnetic and thermal history of the alloys as well as comprehensive information on the nearest environment of a magnetic ion, exchange mechanisms, and local anisotropy.

The distinctive properties of amorphous rare-earth alloys not found in their crystalline analogs of the same composition are as follows:

(1) Even though the giant local anisotropy of rare-earth ions does not result in the occurrence of macroscopic anisotropy because of the random character of the magnetic-ion environment, it does determine the directions of local easy axes and exerts a profound effect on magnetization processes.

(2) The large fluctuations of exchange integrals in amorphous alloys and the existence of competitive exchange interactions opposite in sign reveal themselves in significantly differing values of the Curie temperatures for amorphous alloys and their crystalline analogs with the same chemical composition.

(3) Amorphous alloys exhibit a great variety of magnetic structures and phase transitions.

A S Andreenko, S A Nikitin M V Lomonosov Moscow State University, Vorob'evy Gory, 119899 Moscow, Russia
Tel. (7-095) 939 29 12
Fax (7-095) 932-88 20
E-mail: asa@ofef264a.phys.msu.su

Received 14 November 1996, revised 10 February 1997
Uspekhi Fizicheskikh Nauk **167** (6) 605 – 622 (1997)
Translated by V V Matveev; edited by S N Gorin

(4) The possibility of producing amorphous alloys over a wide range of concentrations as well as the wide selection of dopants provide a unique possibility to smoothly modify their basic magnetic parameters.

(5) The ease of fabrication of amorphous alloys and their good mechanical characteristics offer promise for their practical use.

(6) Magnetoelastic effects in amorphous alloys can show essential peculiarities since they are determined not only by the values of exchange integrals, but also by the 'rigidness' of atomic bonds.

Here we present a review of the latest investigations of the magnetism of bulk amorphous rare-earth materials. Beyond the scope of this review are a number of questions that have been discussed recently in monographs and comprehensive reviews. Among these are the problems of producing amorphous alloys [7–13] and various aspects of their practical application [10–14].

The results of research on thin magnetic films are also omitted from consideration. To offer a satisfactory explanation of the magnetic properties of these films, the peculiarities of magnetic behavior of surface layers and layers adjacent to the substrate must be taken into account. The data obtained in experiments on massive samples several tens of microns in thickness alone are presented and discussed in this review. Such samples can be considered as bulk three-dimensional samples.

2. Magnetic properties, magnetization and magnetization reversal processes in amorphous RE–TM alloys

The following three types of exchange interactions are essential to the analysis of magnetic properties of amorphous RE–TM alloys: the d–d exchange, which is responsible for magnetic ordering at temperatures $T < \Theta$; the f–d exchange, which causes the magnetic moments of rare-earth ions to polarize in an effective exchange field produced by the d-sublattice; and the f–f exchange, which is usually much less than the other two and in many cases can be neglected. It should be noted that all possible types of exchange interactions — direct exchange, superexchange interactions via ligands, indirect exchange via conduction electrons — depend strongly on the distance between interacting ions [15] and, in view of the fluctuations of interatomic distances inherent in amorphous alloys, exhibit marked variations in sign and magnitude.

Structurally disordered materials generally do not have to exhibit a macroscopic anisotropy with a fixed direction of easy axis.† However, high local magnetic anisotropy can arise due to the electrostatic interaction of the high-anisotropic 4f subshell with the local crystal field of neighboring ions. As a result of the fluctuations of the local environment of 4f ions, the direction of the local easy magnetic axis varies randomly from one site to another with some correlation.

Thus, the basic magnetic properties of amorphous alloys under consideration, such as magnetic structures, phase transitions, magnetization and magnetization reversal processes, are determined by the competition of exchange interactions and the local magnetic anisotropy. All the amorphous alloys can be divided into two groups: *high-anisotropy alloys*, in which random magnetic anisotropy highly dominates over the exchange interaction, and *low-anisotropy alloys* with a rather weak random anisotropy as compared to the exchange interaction. These two groups of alloys have different magnetic properties. However, there is no strict dividing line between them, because their properties depend strongly on the component/concentration ratio. Consider in this context the principal experimental facts and theoretical concepts developed in the last few years.

† Except for alloys in which a uniaxial or unidirectional anisotropy can be induced due to special conditions of fabrication or heat treatment. The effects of induced anisotropies on the magnetic properties will be discussed in Section 3.

2.1 Magnetization processes in high-anisotropy alloys

Consider the magnetic properties of amorphous Er_xFe_{100-x} alloys with $x = 26$, 32 and 54 at.%. Measurements have shown that these alloys exhibit no magnetic anisotropy [16]. In none of these alloys has magnetic ordering been found at room temperature (they are paramagnets). The investigation of the temperature dependence of magnetization was conducted in the following manner. The initial magnetic state of an alloy was produced by cooling a sample to a temperature of 4.2 K. Cooling was carried out in two ways: (1) without magnetic field and (2) in a magnetic field. Thereafter measurements of the temperature dependence of magnetization were made. Henceforth, the commonly accepted terminology will be used: when a sample is cooled without a magnetic field, the process is referred to as ZFC (zero field cooled), otherwise it is referred to as FC (field cooled). Hysteresis loops and magnetization curves were recorded upon demagnetization of a sample at the measurement temperatures.

Lowering the temperature resulted in magnetic ordering. Figure 1 shows the hysteresis loops and magnetization curves of the $Er_{26}Fe_{74}$ alloy at various temperatures. The width of

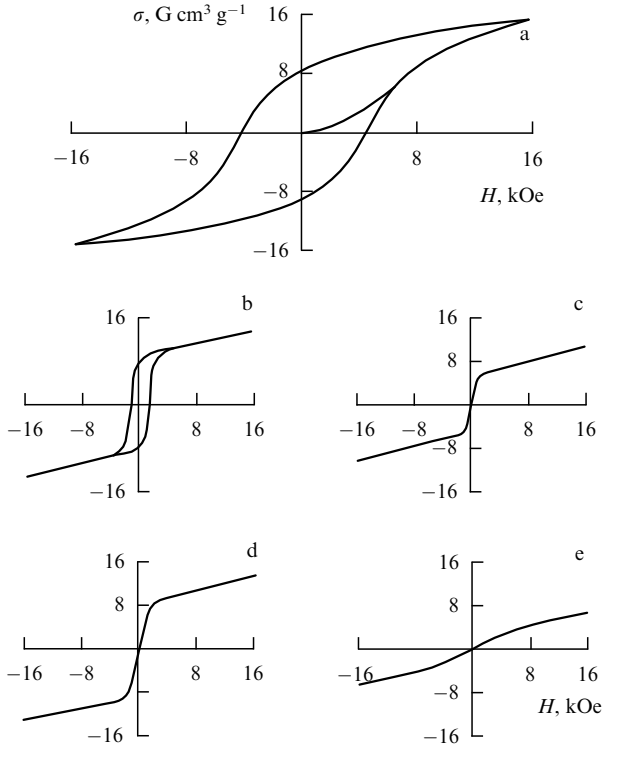

Figure 1. Hysteresis loops and initial magnetization curves for the amorphous $Er_{26}Fe_{74}$ alloy at different temperatures: (a) 28; (b) 65; (c) 104; (d) 185; and (e) 250 K.

the hysteresis-loop and the coercive force increase sharply with decreasing temperature.

Figure 2 illustrates the temperature dependence of magnetization $\sigma(T)$ (in ZFC and FC modes) and magnetic susceptibility $\chi(T)$. As is seen from this figure, a rise in magnetization of alloys associated with magnetic ordering is observed as the temperature decreases. About the same value of the Curie temperature was obtained from measurements of the temperature dependence of magnetic susceptibility (see Fig. 2).

A sharp decrease in the Curie temperature of amorphous Er – Fe alloys with decreasing Fe content testifies to the fact that the d – d exchange is the dominant exchange interaction in these alloys. The smooth variation of specific magnetization near the Curie temperature is evidence of a 'smeared' phase transition with large local fluctuations of magnetic anisotropy energy [17].

In all amorphous Er – Fe alloys, a maximum in the temperature dependence of magnetization $\sigma(T)$ was observed below the Curie point in the temperature range 30 to 100 K. The temperature corresponding to this maximum was strongly dependent on the magnitude of the magnetic field in which a sample was warmed. On the inset in Fig. 2, the temperature dependence of the magnetic field H_m corresponding to a maximum of $\sigma(T)$ is presented. For comparison, a curve for the temperature dependence of the coercive force H_c is also presented.

It is noteworthy that everywhere over the temperature region the coercive force is markedly less than the magnetization-maximum field H_m. This indicates that the coercive force H_c and the field H_m are determined by different mechanisms.

For the amorphous magnets, the problem of magnetic-state determination reduces to a variation problem where the coefficients of the thermodynamic potential density are stochastic functions. The moments of these quantities (means, variances, correlation functions, and so on) need to be given in a phenomenological form or as model parameters. The situation is complicated by the absence of small parameters which could be used for linearization and simplification of the nonlinear differential Euler – Lagrange equations.

As is known, the original magnetic state of amorphous RE – TM alloys is a macroscopically disordered structure. However, small regions of a sample can make up a peculiar kind of domain structure. This structure is chaotic in the sense that the orientations of the magnetization vectors of domains are random. The possibility of the occurrence of such structures in strongly fluctuating systems was indicated by Imry and Ma [17]. The domain sizes are determined by the competing magnetostatic and exchange interactions as well as anisotropy effects, which predominantly affect the orientation of the domain magnetization. On application of an external magnetic field, a realignment of the domain structure takes place, which results in the appearance of macroscopic magnetization. Such an assumption is supported by the large coercivity and small domain-wall mobility, indicating the existence of a large number of scattering and trapping centers as well as the non-180° nature of domain walls.

The thermodynamic potential of the ith domain can be written in the form [16]

$$\Phi_i = -M'(T)H\cos\varphi_i - K(T)\cos^2(\varphi_i - \psi_i)\,, \qquad (1)$$

where $M'(T)$ is the domain magnetization, $K(T)$ is the magnetic anisotropy constant, φ_i and ψ_i are the angles the external magnetic field $\mathbf{H}$ makes with the magnetization vector and the anisotropy axis of the domain, respectively.

The magnetic states of a system are determined through the minimization of Eqn (1) with respect to the angles, taking into account the stability conditions for the solutions obtained. Actually, the problem reduces to the study of the magnetization process for a ferromagnet in an inclined magnetic field followed by summation over all domains and averaging over the angle ψ that specifies the directions of the easy axes of these domains. On the assumption that in the

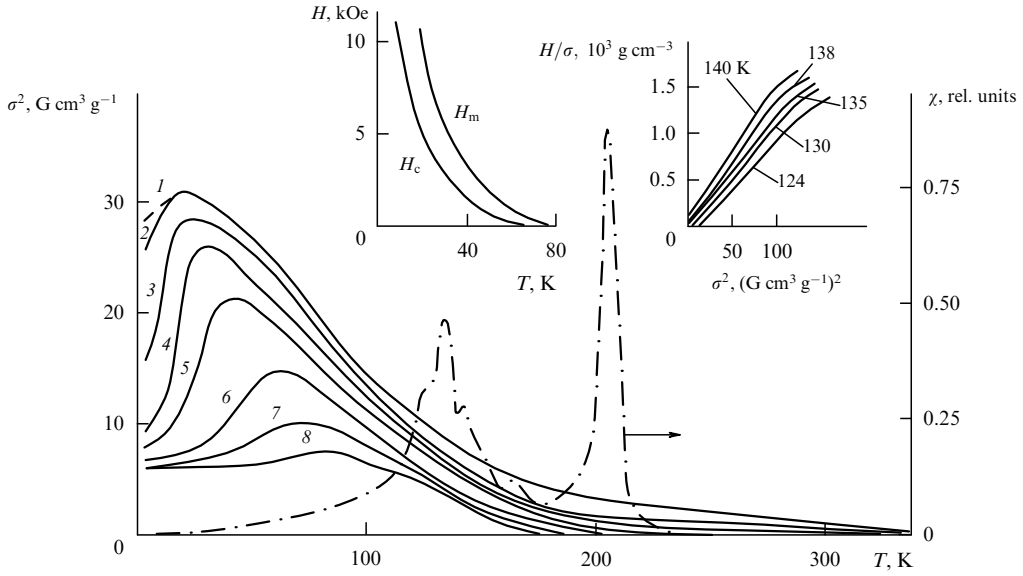

Figure 2. Temperature dependence of specific magnetization for an amorphous alloy. Curve *1* was obtained on heating in a field $H = 14$ kOe after cooling in a field of 14 kOe. The curves *2* – *8* for the ZFC magnetization were obtained on warming-up in the following fields: (*2*) 14 kOe, (*3*) 10 kOe, (*4*) 6 kOe, (*5*) 3 kOe, (*6*) 1 kOe, (*7*) 0.5 kOe, (*8*) 0.2 kOe. The $\chi(T)$ dependence is shown by the dashed line. On the insets: the $H_c(T)$ and $H_m(T)$ dependences and the $H/\sigma(\sigma^2)$ dependence.

absence of a magnetic field the domain magnetization vectors are distributed over directions with a constant probability density (uniformly 'fill' the sphere), the total magnetization per formula unit can be written as follows:

$$I = \frac{M'(T)}{2} \int_0^{\pi} \cos\bigl[\varphi(\psi, H, T)\bigr] \sin\psi \, \mathrm{d}\psi \,. \tag{2}$$

Such a structure may occur in amorphous films of reasonable thickness (several tens of microns), where no 'thin-film' peculiarities of the magnetic state are observed.

According to the Harris – Plischke – Zuckermann model [18], the crystalline-field Hamiltonian for rare-earth ions in an amorphous matrix can be written in the form

$$\overline{H}_{\mathrm{cryst}} = -D \sum_i \bigl(\widehat{J}_{z_i}^{(i)}\bigr)^2 \,, \tag{3}$$

where $\widehat{J}^{(i)}$ is the magnetic moment of the ith ion, the summation is performed over all f ions, $D > 0$ is a constant which is the same for all sites. The orientation of the z_i axis varies from one site to another. This model adequately describes the properties of amorphous alloys based on rare-earth metals.

It has been found experimentally [15] that the exchange interaction between rare-earth and 3d transition ions is much less than the d – d exchange. Therefore, the f subsystem may be thought of as a paramagnet placed in an effective field which is the sum of an external field and an effective f – d exchange field.

Leaving aside the mathematics (see [16]), we write only the final expression

$$\frac{\Phi_i}{K(T)} = -\beta \cos\varphi - \cos^2(\varphi - \psi) \,, \tag{4}$$

in which

$$\beta = \frac{H}{K_0 M_0} \frac{1 - \tau}{\tau^{\delta}} \,, \tag{5}$$

where M_0 and K_0 are the magnetization and the anisotropy constant at $T = 0$, respectively, $\tau = 1 - T/\Theta$, Θ is the Curie temperature, and δ is a dimensionless parameter.

An important feature of this model is that the parameters δ, K_0, M_0, and T describing the magnetic properties of an amorphous alloy enter into the final expression (4) in the form of a universal combination specified by a dimensionless parameter β. Minimization of the thermodynamic potential (4) gives the following equation for determining the angle:

$$\beta \sin\varphi = \sin\bigl[2(\varphi - \psi)\bigr] \,. \tag{6}$$

This equation in combination with the stability condition allows one to solve the problem.

Equation (6) has ambiguous solutions. At $H = 0$, for example, there exist two stable solutions: $\varphi_1 = \psi$ and $\varphi_2 = \psi + \pi$. When applying a magnetic field, one of these solutions (φ_1 at $\psi > \pi/2$ or φ_2 at $\psi < \pi/2$) becomes metastable and lose stability at the β values determined from the equation

$$\cos^{2/3}\psi + \sin^{2/3}\psi = (2\beta^{-1})^{2/3} \,. \tag{7}$$

By analyzing the stability condition (7), one can distinguish three regions of magnetic states:

(a) $\beta < 1$ — low fields or high temperatures. The magnetization process consists in a smooth rotation of the domain magnetization vectors.

(b) $1 < \beta < 2$ — an intermediate region, in which the domain magnetization vectors with $\psi > \pi/2$ change their orientation. The magnetization process becomes irreversible and a sharp increase in magnetization is observed.

(c) $\beta > 2$ — the magnetization jumps are completed and the magnetization vectors of domains tend toward the direction of the external magnetic field. The magnetization falls as the Curie point is approached.

Equation (6) [along with Eqn (7)] can be solved for all these regions using numerical methods. A typical result of such calculations is presented in Fig. 3 (curve *3*). The regions of magnetic states corresponding to the cases a, b and c are outlined in this figure by dashed lines. A smooth change-over from one state to another with changes of temperature and the maxima in the $\sigma(T)$ curves measured in a fixed magnetic field are worthy of notice. It is seen from Fig. 3 that the best agreement between theory and experiment is observed in the intermediate temperature region. Discrepancies at low temperatures may be due to the higher-order anisotropy terms in the expansion of the thermodynamic potential, which are not accounted for in the simple model and may modify the temperature dependence of the anisotropy. Discrepancies in the high-temperature region are attributable to the use of simple power functions for describing a two-sublattice magnet with a complex temperature dependence of magnetic parameters for each sublattice.

An analysis of the temperature dependences of the coercive force and the magnetization-maximum field reveals the following. The major hysteresis loop corresponds to the remanent magnetization of domains whose magnetic moments 'fill' a half-sphere. For a magnetic field applied in

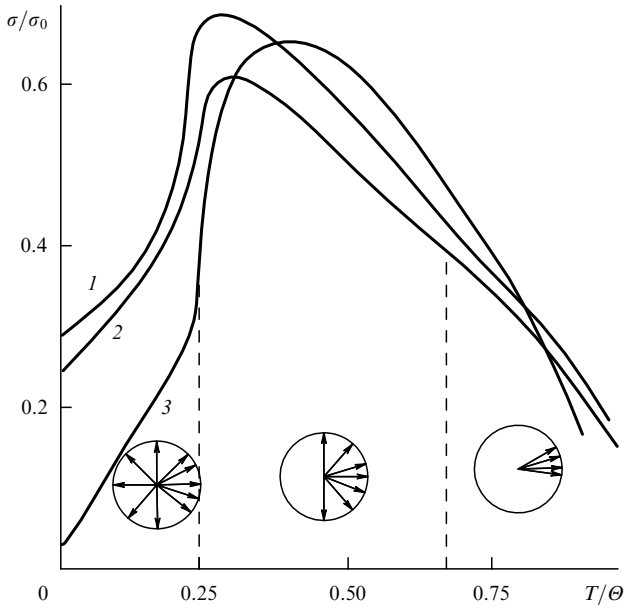

Figure 3. Experimental (curve *1* for the $Er_{32}Fe_{68}$ alloy and curve *2* for the $Er_{54}Fe_{46}$ alloy) and calculated (curve *3*) temperature dependences of the ZFC magnetization on heating in a field $H = 3$ kOe. The arrangement of the magnetic moment of domains in various temperature regions is shown schematically.

the opposite direction, one can find a field magnitude providing zero magnetization. This point corresponds to the onset of the jumpwise changes of the magnetic moments of the domains. At not-too-high temperatures, the magnetization-maximum field $M(T)$ corresponds to $\beta = 2$ (the completion of the jumping processes). As a result, $H_m(T) \simeq 2H_c(T)$, and this provides an explanation for the experimental data presented in Fig. 2. At high temperatures, the temperature dependence of magnetization compensates its rise through rotation. The values of H_c and H_m come close together as the temperature increases because of the faster decrease of H_m with temperature.

Experimental magnetic parameters of amorphous alloys were used in calculations of a hysteresis loop (Fig. 4). As is seen from Figs 3, 4, there is good qualitative agreement between theory and experiment.

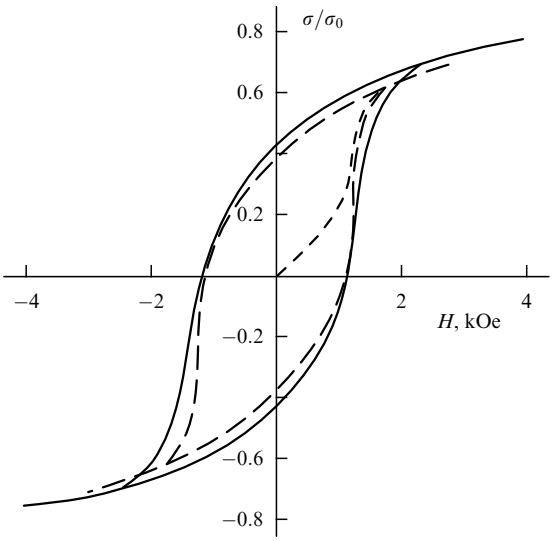

Figure 4. Experimental (solid line) and calculated (dashed line) hysteresis loops for the $Er_{32}Fe_{68}$ alloy at $T = 37$ K.

An analysis of experimental data carried out for several systems of amorphous alloys showed [19] that the magnetic properties of alloys such as Er_xFe_{100-x} $(26 \leqslant x \leqslant 54)$, Dy_xCo_{100-x} $(26 \leqslant x \leqslant 56)$, Tb_xFe_{100-x} $(46 \leqslant x \leqslant 70)$, Tb_xCo_{100-x} $(26 \leqslant x \leqslant 40)$ may be satisfactorily described by this model.

However, some initial assumptions used in the model discussed above may not be true in actual practice. For example, increasing 3d metal content may result in breaking of the spherical symmetry of the distribution of domain magnetization vectors. In addition, it is reasonable to assume the existence of a preferred orientation of easy axes (EA) in thick magnetic films, which may result in the convergence of the values of H_c and H_m because of increasing H_c.

In alloys with a high content of 3d metal, the random magnetic anisotropy energy becomes much less than the exchange energy. Therefore, such alloys may be assigned to low-anisotropy amorphous alloys.

2.2 Magnetization processes in low-anisotropy alloys

Figure 5 illustrates the temperature dependence of magnetization for the $Tb_{21}Co_{79}$ alloy measured in the ZFC mode. The $\sigma(T)$ curves differ substantially from those for high-anisotropy alloys. First, the H_m and H_c values are virtually the same, which is seen from the inset in Fig. 5. Second, the magnitudes of the magnetic fields used in the experiments are sufficient to destroy the spin-glass state. A comparison of the hysteresis loops (Fig. 6) also testifies that the magnetization processes in the high-anisotropy and low-anisotropy alloys differ noticeably. This shows up in the decrease of the coercive force and in the zero slope of the magnetization curve in high fields (cf. the curve *1* for a low-anisotropy alloy with curve *3* for a high-anisotropy alloy). The investigation of domain structures in alloys with a high content of 3d metal revealed the existence of a periodic stripe-domain configurations [20]. Local magnetic anisotropy of each rare-earth ion does not change with decreasing concentration of these ions. However,

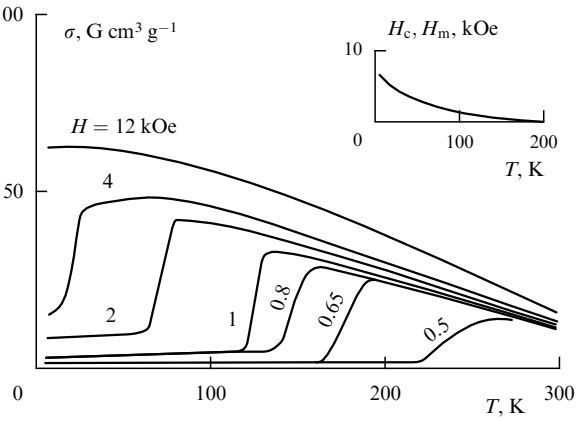

Figure 5. Temperature dependences of specific magnetization $\sigma(T)$ for the amorphous $Tb_{21}Co_{79}$ alloy on heating samples in magnetic field after ZFC. Field values are given at the curves. The inset displays the $H_c(T)$ and $H_m(T)$ dependences.

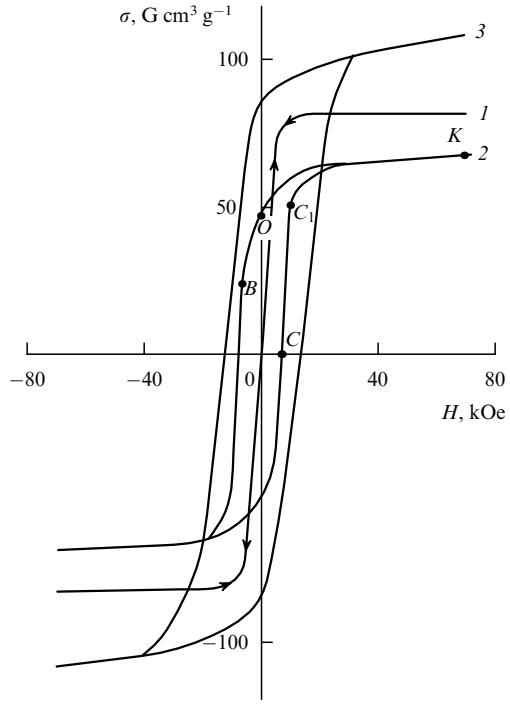

Figure 6. Hysteresis loops for the amorphous alloys $Tb_{10}Co_{90}$ (*1*), $Tb_{26}Co_{74}$ (*2*) and $Tb_{34}Co_{66}$ (*3*) at $T = 1.5$ K.

the total number of RE ions decreases, which results in the decreased contribution of random magnetic anisotropy to the total magnetic energy of an alloy. As a result, a displacement of domain walls becomes possible in contrast with high-anisotropy alloys in which such walls are practically absent.

The results reported in papers [21, 22] were used for describing magnetization and magnetization reversal processes in amorphous alloys with a high content of 3d metal.

In the simplest approximation, with allowance for structural fluctuations that result in fluctuations of the crystal field acting on rare-earth ions, the free energy of a system can be written in the form

$$\Delta F_{\mathrm{R}} = \frac{\hat{\chi}(T)}{2}(H + H_{\mathrm{eff}})^2 , \qquad (8)$$

where $\hat{\chi}$ is the tensor of paramagnetic susceptibility of the rare-earth ion, $H_{\mathrm{eff}} = -I_{\mathrm{fd}} M_{\mathrm{TM}}$ is the effective exchange field acting on the RE ion from the d subsystem, I_{fd} is the f–d exchange parameter, and M_{TM} is the magnetic moment of the 3d metal. This magnetic moment is convenient to use as the independent variable in the free energy of a system when considering the magnetic properties of RE–TM alloys [23]. The contribution of RE ions results in the appearance of magnetic anisotropy whose values increase with decreasing temperature because of a hyperbolic rise of $\chi(T)$.

Leaving aside the detailed analysis of the model (see Ref. [24]), we will consider the main conclusions from it. It was shown that because of the large value of local anisotropy, which is determined predominantly by the contribution of the RE ions, the wall coercive force H_{c} is also high, so that the fact of the non-increase of magnetization in magnetic fields $H < H_{\mathrm{c}}$ is attributable to the retention of domain-wall displacements (Fig. 6). Applying a magnetic field results in changes of the dispersion D_{m} of orientational fluctuations and, hence, the magnitudes of the average magnetic moments of domains. However, an increase the magnetic field is not accompanied by the increase of the total magnetic moment of a sample, since D_{m} decreases only in the domains whose magnetization has a positive projection on the direction of the magnetic field. If this projection is negative, D_{m} increases. Thus, the average magnetic moment of a sample with an arbitrary orientation of magnetization in different domains does not change.

At $H > H_{\mathrm{c}}$, a domain wall displacement begins. This process is accompanied by suppressing orientation fluctuations (with decreasing D_{m}). In the samples under investigation the demagnetizing factor is small when a film is magnetized along its plane, so that the wall displacement process occurs in a very narrow range of fields and the corresponding portion of the magnetization curve (see Fig. 6, curve *2*, section CC_1) is almost vertical. On section C_1K, the process of suppressing orientational fluctuations D_{m} is in progress. Previously, this process did not contribute to the total magnetic moment of the sample because of the presence of the domain structure. To the right of point C_1 on the curve CC_1K, the sample is in the single-domain state, but fluctuations increase with decreasing magnetic field and this results in a decrease of the total magnetic moment of the sample (section KO).

On inversion of the magnetic field (section OB), the orientational fluctuations continue to rise. As a result, the probability of appearance of rather large regions in which the magnetic moment makes an obtuse angle with the magnetic-field direction is increased. Such regions play the role of nuclei for magnetization reversal.

A large value of the wall coercive force is responsible for the temperature dependence of the sample magnetization and its magnetic history. Because of small demagnetizing fields, the sample cooled in an external magnetic field remains in a single-domain state upon turning this magnetic field off. In this case, an increase in magnetization on heating is due to suppression of orientational fluctuations in a nearly single-domain sample because of the decrease of the magnetic anisotropy constant.

If a sample is demagnetized at $T = 0$, a considerable increase in its magnetization (found experimentally) is attributable to a domain wall displacement in a fixed field $H = H_{\mathrm{c}}(T)$ (see Fig. 6).

Thus, it may be thought of as experimentally established fact that it is the relationship between the random magnetic anisotropy energy and the exchange energy that is the main factor determining the magnetization and magnetization reversal processes in amorphous RE–TM alloys. Since the random magnetic anisotropy energy is determined mainly by the RE ion content and the exchange energy is determined by the 3d transition-metal content, the magnetization processes are unambiguously determined by the RE–TM concentration ratio. In alloys rich in RE ions magnetization processes are effected predominantly through a rotation of the magnetization vectors of domains, while in alloys with a high content of transition metal, they are due to domain-wall displacement. A direct correlation between interatomic distances and magnetization processes is also observed [19].

3. Effect of induced magnetic anisotropy on magnetization processes

Along with random local magnetic anisotropy, some amorphous alloys exhibit induced macroscopic magnetic anisotropy. There are two methods to induce this anisotropy: applying an external magnetic field during thermal treatment of a sample and using special techniques during sample fabrication (sputtering in an external magnetic field, for example). The value of the induced magnetic anisotropy may be as great as 10^7 erg cm^{-3} [25]. The former approach has received the most study. Here, an external magnetic field provides a preferred direction in a previously isotropic magnet and brings into existence remanent magnetization. This approach will not be discussed in this review. The second approach merits detailed analysis since no detailed investigations of its related physical mechanism are available. The anisotropy induced during sample fabrication significantly affects the magnetization processes in amorphous alloys.

Depending on the conditions of sputtering, the anisotropy axis may lie either in the plane of a film [26–30] or perpendicular to this plane [26–28, 31–40]. There exist several experimental techniques to induce microscopic anisotropy during sample fabrication and monitor its magnitude and direction: sputtering in a constant magnetic field [28, 36–40], variation of the substrate temperature [25–27, 37], changing argon pressure during ion-plasma sputtering [29, 31, 40], sputtering using two argon beams [34], applying a negative bias to the substrate [27, 28, 30–34], and combinations of these methods.

In spite of the fact that macroscopic anisotropy is of considerable importance, in particular for producing magneto-optic recording media, so far not much is known about its origin in amorphous alloys. Nevertheless, worthy of mention are a number of papers where some microscopic

and macroscopic mechanisms of its origin were studied. In these papers, data are presented that offer an explanation for macroscopic magnetic anisotropy with invoking such mechanisms as the appearance of a compositional directional short-range order and anisotropy of bond-orientation distribution [41], a repeated evaporation of atoms from the surface of a film during sputtering [42], and the appearance of some pseudodipolar short-range atomic order [42].

Consider some experimental results [24, 43] giving a better insight into the specific magnetic properties of amorphous rare-earth alloys with induced magnetic anisotropy.

When depositing, amorphous alloys were subjected to an external magnetic field $H \simeq 50$ Oe, with the result that macroscopic anisotropy and the easy axis (EA) along this field were induced in them. Figure 7 presents magnetization curves for the amorphous $Tb_{26}Co_{74}$ alloy at different orientations of the magnetic field in the film plane. As is seen from this figure, curve *5*, corresponding to the field aligned parallel to the EA, lies well above the curve measured in a field that is perpendicular to the EA, or parallel to the HA (hard axis). Using EA and HA magnetization curves, one may calculate the magnetic anisotropy energy

$$E_{\text{an}} = \int_{\text{EA}} H\,\mathrm{d}I - \int_{\text{HA}} H\,\mathrm{d}I, \tag{9}$$

which was found to be 4.7×10^5 erg cm^{-3} (dI is the change in the magnetization of the sample in field H).

The results obtained may be explained based on a model that takes into account contributions to the free energy of a magnetic system from the fluctuations of the crystalline field acting on magnetic ions and from the local and induced anisotropy. The magnetic moment M_{TM} of the 3d transition metal is convenient to use as an independent variable [23]. The orientational fluctuation $\delta\mathbf{m}$ of the vector $\mathbf{M}_{\text{TM}}$ is defined as (Fig. 8a)

$$\delta\mathbf{m} = \mathbf{M}_{\text{TM}}(\mathbf{r}) - \langle \mathbf{M}_{\text{TM}} \rangle\,, \tag{10}$$

where $\mathbf{M}_{\text{TM}}(\mathbf{r})$ is the magnetic moment of transition metal atoms located at the point $\mathbf{r}$.

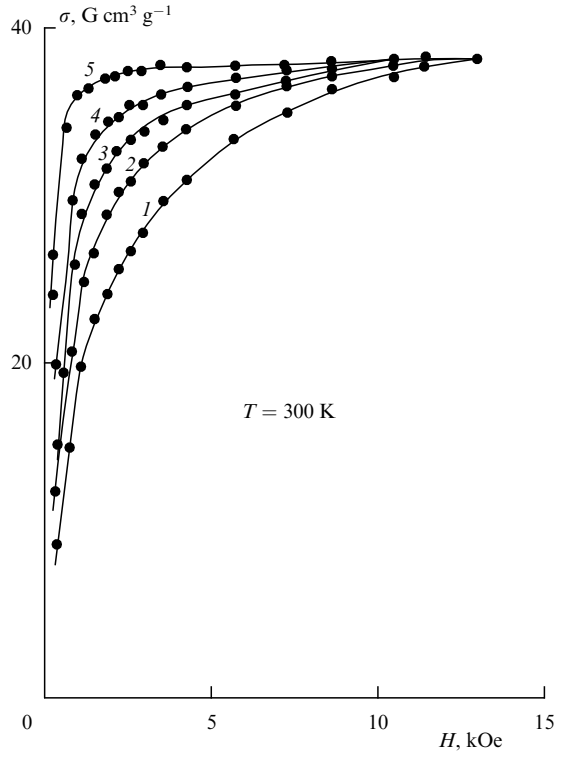

Figure 7. Magnetization curves of amorphous $Tb_{26}Co_{74}$ alloy for different magnetic field directions in the film plane: *1*, magnetic field along HA; *2*, *3*, *4*, *5*, magnetic field at angles 20°, 30°, 40°, 90° to HA, respectively.

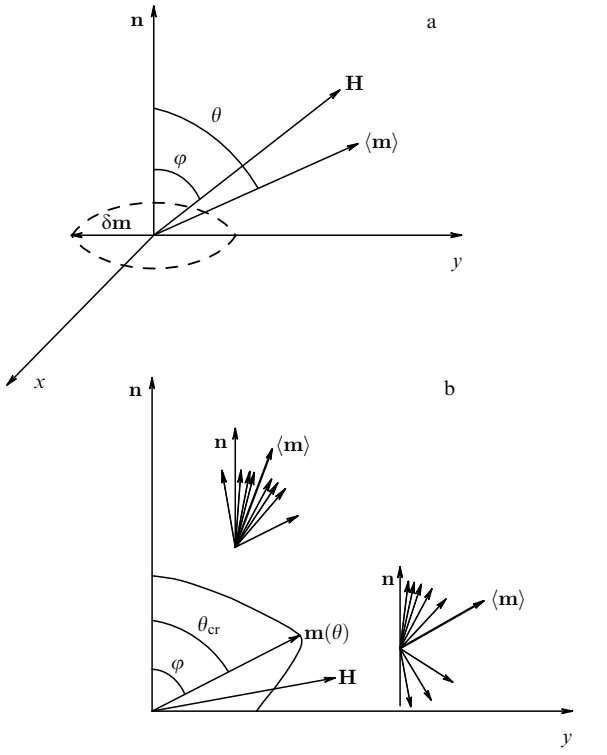

Figure 8. (a) Relative orientation of the induced anisotropy axis $\mathbf{n}$, the magnetic field $\mathbf{H}$, the average magnetic moment of the 3d sublattice $\mathbf{m}$ and its fluctuations $\delta\mathbf{m}(\mathbf{r})$. (b) Dependence of the magnitude of the average magnetic moment $\mathbf{m}(\theta)$ from its orientation. On the insets, the effect of induced magnetic anisotropy on the orientational fluctuations of magnetic moments in the vicinity of EA ($\theta \sim 0$) and HA ($\theta \sim \pi/2$) is illustrated.

The local uniaxial anisotropy energy can be written in the form [19]

$$F_{\text{an}} = -\frac{\beta_{\text{l}}(T)}{2}(\mathbf{M}_{\text{TM}} \cdot \mathbf{l})^2\,, \tag{11}$$

where $\mathbf{l}$ is the unit vector specifying the orientation of a local anisotropy axis. No long-range order in the $\mathbf{l}(\mathbf{r})$ arrangement is present, and the correlation function has the form

$$K_{\alpha\beta}(\mathbf{r}, \mathbf{r}') = \langle \mathbf{l}_\alpha(\mathbf{r}) \cdot \mathbf{l}_\beta(\mathbf{r}') \rangle - \langle \mathbf{l}_\alpha(\mathbf{r}) \rangle \cdot \langle \mathbf{l}_\beta(\mathbf{r}') \rangle$$
$$= \langle \mathbf{l}_\alpha \cdot \mathbf{l}_\beta \rangle \exp\left(-\frac{|\mathbf{r} - \mathbf{r}'|}{R_{\text{c}}}\right).$$

The symbol $\langle \ldots \rangle$ indicates averaging over the $\mathbf{l}(\mathbf{r})$ fluctuations. the constant β_{l} is determined by the contributions from both the rare-earth and 3d sublattices.

The unit vectors $\mathbf{l}(\mathbf{r})$ specifying the orientation of the local anisotropy axes may possess a preferred orientation $\mathbf{n}$, and it is this that causes the appearance of induced magnetic anisotropy.

Leaving aside the mathematics associated with the derivation of the expression for the average magnetic moment of a system, we write the final formula [24]

$$\left|\langle\mathbf{m}\rangle\right| \equiv m(\theta) = \left\langle \mathbf{M}_{\mathrm{TM}}(\mathbf{r}) + \mathbf{M}_{\mathrm{R}}(\mathbf{r})\right\rangle$$

$$= \left|(1 + \langle\chi_0\rangle J_{\mathrm{fd}})\right| m_0 \left[1 - \frac{D_{\mathrm{m}}(\theta)}{2m_0^2}\right], \qquad (12)$$

where $\chi_0(T)$ is the isotropic part of the magnetic susceptibility tensor, J_{fd} is the f–d exchange integral, θ is the angle between the easy axis and the $\mathbf{M}_{\mathrm{TM}}$ direction, $\mathbf{M}_{\mathrm{R}}(\mathbf{r})$ is the magnetic moment of the rare-earth ion, and $M_{\mathrm{TM}} = m_0 \equiv \mathrm{const}$.

It follows from this expression that the magnitude of the average magnetic moment of a system depends on its orientation determined by the angle θ. As is shown in Fig. 8b, this magnitude $m(\theta)$ decreases as the magnetic moment approaches HA. This effect is due to induced anisotropy, which suppresses the orientational fluctuations of $M_{\mathrm{TM}}(\mathbf{r})$ if $\langle\mathbf{m}\rangle$ is close to $\mathbf{n}$ and enhances them if $\langle\mathbf{m}\rangle$ is close to HA. In systems with induced anisotropy, the specific $m(\theta)$ dependence brings into existence regions of forbidden orientations for the vector $\langle\mathbf{m}\rangle$. For example, the rotation of $\langle\mathbf{m}\rangle$ toward the field direction through an angle greater that θ_{cr} would be accompanied by a decrease in the Zeeman energy of the system and hence is impossible. Thus, on the final section of the magnetization curve the rotation of the average magnetic moment slows down since a portion of the magnetic field energy is expended not on the rotation of $\langle\mathbf{m}\rangle$, but on the suppression of orientational fluctuations of $\mathbf{M}_{\mathrm{TM}}(\mathbf{r})$ (decreasing D_{m}). This effect is illustrated in Fig. 9 where the field dependence of the angle between $\langle\mathbf{m}\rangle$ and the external magnetic field $\mathbf{H}$ calculated using the experimental data presented in Fig. 7 is shown. Since the rotation rate of $\langle\mathbf{m}\rangle$ slows down in the vicinity of HA, the angle between $\langle\mathbf{m}\rangle$ and $\mathbf{H}$ increases in contrast with ordinary ordered magnets, where it decreases.

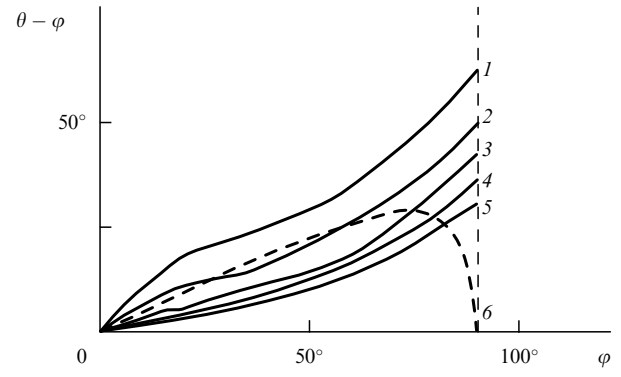

Figure 9. Dependence of the angle $\theta - \varphi$ between the average magnetic moment of the $Tb_{26}Co_{74}$ alloy and the constant-in-magnitude field $\mathbf{H}$ from the field orientation $\mathbf{H}(\varphi)$ calculated using data of Fig. 7: (*1*) $H = 1$ kOe, (*2*) 2 kOe, (*3*) 3 kOe, (*4*) 4 kOe, (*5*) 5 kOe. For comparison, the data for an ordered uniaxial ferromagnet in field $H < \beta_1/m_0$ are presented (curve *6*).

The peculiarities of the angular dependence of the average magnetic moment of a sample result in specific anomalies in the torque-moment curves. Figure 10 presents the torque moment curves for the amorphous $Tb_{21}Co_{79}$ alloy measured at a temperature of 99 K. Such measurements were conducted in magnetic fields directed along the plane of the sample. As is

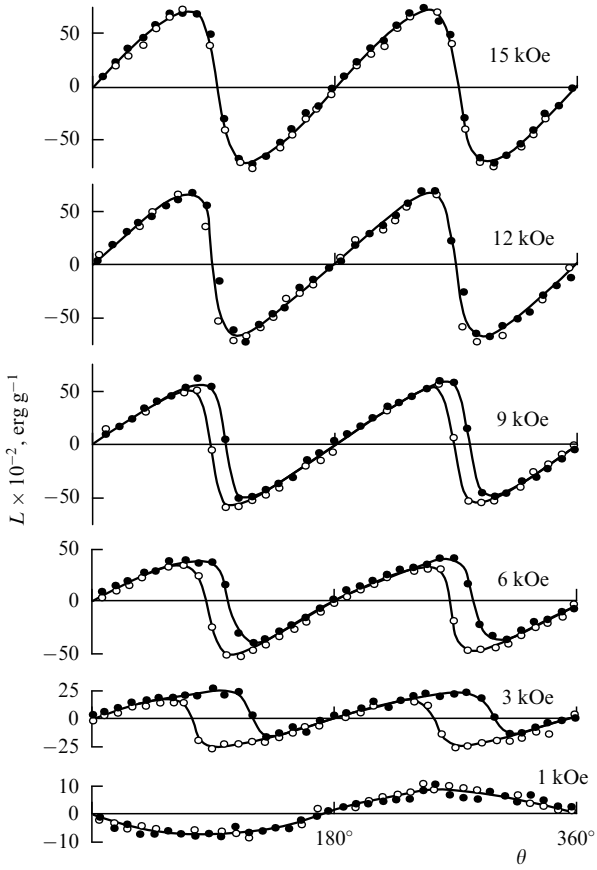

Figure 10. Angular dependences of torque moment for the amorphous $Tb_{21}Co_{79}$ alloy at $T = 99$ K in different magnetic fields (their magnitudes are indicated on the figure).

seen from the figure, in fields greater than the coercive force H_{c} ($H_{\mathrm{c}} = 2$ kOe at $T = 99$ K), the curves have a period of 180°, which was to be expected in the case of uniaxial magnetic anisotropy. At $H < H_{\mathrm{c}}$ the period is equal to 360°, since the magnetic moment of an alloy cannot overcome an energy barrier and invert its direction.

The $L(\theta)$ curves show characteristic abrupt jumps in the vicinity of the angle $\theta = \theta_{\mathrm{cr}}$. Such jumps are observed both in measurements of torque moments starting from small angles and in 'reverse' measurements, starting at large angles. Hysteresis of the $L(\theta)$ curves has also been found in magnetic fields $H \leqslant 9$ kOe.

The torque moment $L_{\max}(H)$ for this alloy measured at various temperatures is linear in H in the initial portion of the $L_{\max}(H)$ curves and slows down its rate of increase in higher fields.

To explain these experimental results, we make use of theoretical concepts outlined above. From the scheme presented in Fig. 11, it is seen that there exists a region of forbidden (energetically unfavorable) orientations of the average magnetic moment $\langle\mathbf{m}\rangle$. Over a reasonably wide range of fields, the angles θ_{cr} have only a weak dependence on the magnitude of $\langle\mathbf{m}\rangle$ and tend to increase with increasing magnetic field H. This behavior is due to the suppression of fluctuations and, hence, decreasing the local minimum ('gap') in the $m(\theta)$ dependence.

This feature of magnetization processes must lead to a spasmodic change of the torque moment L at $\theta = \theta_{\mathrm{cr}}$ (Fig. 12).

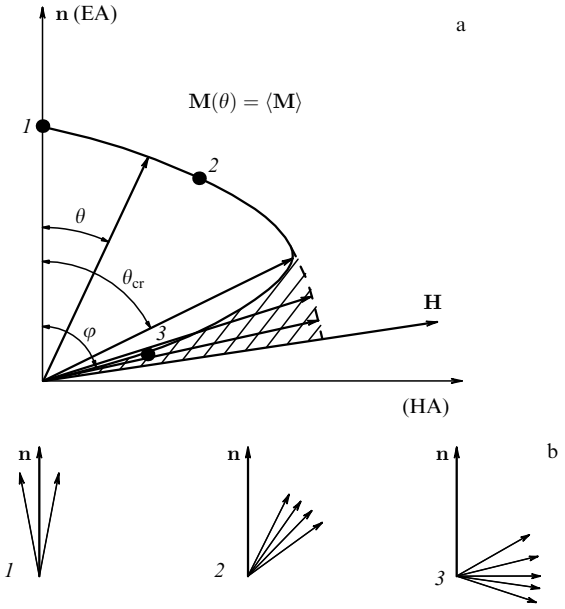

Figure 11. Dependence of the magnitude of the average magnetic moment from its orientation (schematic): (a) the region $\theta > \theta_{cr}$ is 'forbidden', EA and HA are determined by induced anisotropy; (b) dispersion of orientational fluctuations of $m(\theta)$ at different orientations (*1, 2, 3*) of $\langle \mathbf{m} \rangle$.

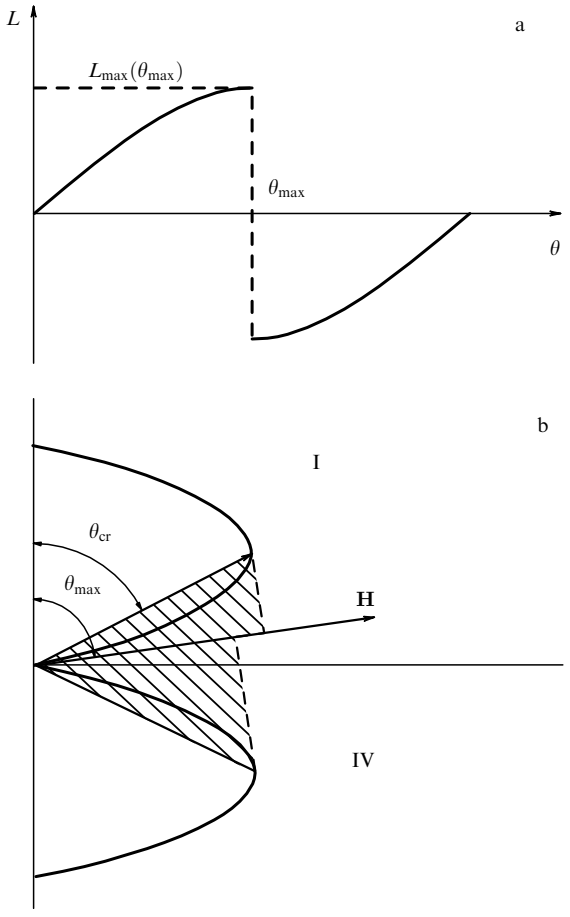

Figure 12. Anomalies in torque-moment curves $L(\theta)$ (schematic): (a) character of the $L(\theta)$ curves; (b) jump of $\langle \mathbf{m} \rangle$ from the first to the fourth quadrant because of the appearance of the regions of forbidden orientations (shaded).

The $L_{max}(H)$ value just before the torque-moment jump (see Fig. 12) can be written in the form

$$L_{max}(H) = m(\theta_{cr}) H \sin(\theta_{max} - \theta_{cr}) . \quad (13)$$

Thus, the results of torque-moment measurements in amorphous Tb–Co alloys are adequately described in the framework of the model presented above.

Of fundamental importance is the question of the value of the induced anisotropy energy and its nature. Estimates carried out for amorphous Tb–Co alloys [43] from the magnetization and torque-moment measurements gave the results which are in close agreement: at room temperature the value of the induced magnetic anisotropy was found to be $\simeq 10^5$ erg cm^{-3}. A comparison with the value of the magnetoelastic energy calculated from the magnetostriction [20] and Young's modulus [44] measurements shows that there is a considerable magnetoelastic contribution ($W_{ME} = 10^4 - 10^5$ erg cm^{-3}) to the induced magnetic anisotropy energy in amorphous Tb–Co alloys.

In the course of the investigation of induced magnetic anisotropy in amorphous Tb–Co alloys, a new effect — the rotation of the easy axis under the action of magnetic field — was found [45, 46]. We consider this effect with the amorphous $Tb_{21}Co_{79}$ alloy as an example. Figure 13 presents hysteresis loops measured in magnetic fields both parallel and perpendicular to EA. As is seen from this figure, these hysteresis loops differ in character and, in particular, exhibit different values of remanent magnetization σ_r.

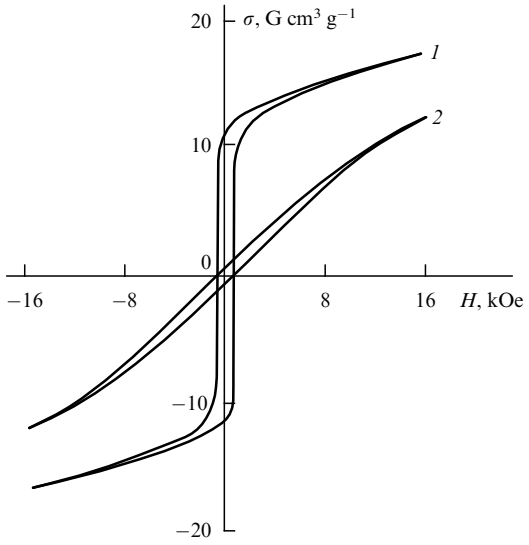

Figure 13. Hysteresis loops in fields aligned with EA (curve *1*) and HA (curve *2*) for the $Tb_{21}Co_{79}$ alloy at $T = 300$ K.

The experimental procedure was as follows. A sample was magnetized along EA in a magnetic field of 16 kOe. Upon turning the field off, the direction of the remanent magnetization $\boldsymbol{\sigma}_r$ was determined by rotating the detection coils. Then, the direction of HA ($\sigma_r = 0$) was determined and a fixed magnetic field in a range of 1 to 16 kOe was applied along HA. Upon turning this field off, the same procedure was used for determining a new direction of EA (induced by turning on the field H aligned with HA). Subsequently, this procedure was repeated for the next value of the field.

The angle $\Delta\varphi$ that the vector $\boldsymbol{\sigma}_r$ makes with its initial direction slowly increases with the magnetic field. At $H > 11$ kOe the rate of change of $\Delta\varphi$ undergoes a sharp increase, and as the field increases further in the range 11 to 16 kOe, this angle approaches 180°. Simultaneously, the magnitude of σ_r changes, passing through a minimum in the vicinity of 11 kOe.

To explain these results, it must be taken into account that $Tb_{21}Co_{79}$ is a compensated alloy: the average magnetic moments of the terbium and cobalt subsystems are nearly equal in magnitude and opposite in direction over a wide range of magnetic ordering [47]. The presence of structural fluctuations inherent in amorphous systems leads to the coexistence of regions where the magnetic moment of Co ions exceeds that of Tb ions, $|\langle M_{Tb}\rangle| < |\langle M_{Co}\rangle|$, and regions where $|\langle M_{Tb}\rangle| > |\langle M_{Co}\rangle|$.

Magnetization processes in these regions differ in character. In the region where $|\langle M_{Tb}\rangle| < |\langle M_{Co}\rangle|$, the magnitude of the average magnetic moment of the alloy depends on its orientation relative to the local EA. A magnetic field applied along the macroscopic EA causes a primary growth of domains whose magnetic moments make an acute angle with the magnetic field. Subsequent magnetizing of a sample perpendicular to the EA results in the turning of the magnetic moment of the Co subsystem and its disordering because of strengthening of orientational fluctuations.

After turning of the magnetic field off, the magnetic moments of the Co ions are confined in the minima of the local magnetic anisotropy energy. As a result, the magnetic moment of the Co subsystem proves to be less than the initial moment and this results in a decrease of σ_r. If the magnetic field H is perpendicular to EA and is sufficiently high, $|\langle M_{Co}\rangle|$ may become less than $|\langle M_{Tb}\rangle|$, that is, the magnetization process in a field perpendicular to EA may lead to a reorientation of the remanent magnetization vector of a sample.

In the regions with $|\langle M_{Tb}\rangle| > |\langle M_{Co}\rangle|$, magnetization processes have no peculiarities since there exist no regions of forbidden orientations for $\langle M_{Tb}\rangle$ [46]. The effect of reorientation of EA is observed through the whole temperature range, and the magnetic field in which this takes place increases with decreasing temperature, which is attributable to an increase in the magnetic anisotropy constant.

4. Magnetoelastic effects in amorphous alloys

The following phenomena are usually assigned to magnetoelastic effects: temperature shifts of phase transitions under the action of stress and pressure, variations of magnetization with pressure ($\Delta\sigma$ effect), and variations of the linear sizes and the volume of the sample under the action of magnetic field (linear and volume magnetostriction). These effects arise from the dependence of exchange interactions, itinerant electron energy, and local magnetic anisotropy on interatomic distances and atomic volume [48]. We consider magnetoelastic effects that are due to variations of atomic volume under the action of pressure and magnetic field: $\Delta\sigma$ effect, Curie-temperature shift, linear and volume magnetostriction. The appearance of new magnetic phases and change in the character of phase transitions under the action of pressure may also be considered as magnetoelastic effects. Experimental and theoretical investigations of magnetoelastic effects allow one to obtain valuable information about the fundamental interactions responsible for magnetic ordering.

The models describing magnetovolume effects are usually based on three approaches. The models based on the localized magnetic moment approximation provide a good explanation for the effect of pressure on the magnetic properties of rare-earth metals and their alloys [48 – 64]. The band model is successfully used for describing the effect of pressure on the magnetic properties of 3d transition metals and their alloys [65 – 70]. The combined model is used for describing the pressure dependence of magnetic properties of RE – TM compounds [71 – 75]. It should be noted that there are only few works on the investigations of magnetovolume effects in amorphous alloys [76 – 85] in contrast with the comprehensive information on the effect of pressure on the magnetic properties of crystalline samples. Moreover, these investigations are not systematic. Only in a few of these works have the pressure dependence of the Curie point [76 – 78] and the $\Delta\sigma$ effect [77 – 79] been investigated.

In this section, the results of the latest investigations on the pressure dependence of the Curie temperature, intra- and interlattice exchange interactions and magnetic phase transitions in amorphous RE – TM alloys [86 – 89] are reported.

4.1 Effect of pressure on the Curie temperature and exchange interactions

When describing the magnetic properties of amorphous RE – TM alloys, it must be taken into account that the values of exchange integrals in these alloys may differ essentially from the corresponding values in crystalline compounds. These distinctions are due to the fluctuations of exchange interactions inherent in amorphous alloys, the redistribution of itinerant-electron density in disordered structures as well as distinctions in the local environment of magnetic ions. Since all these characteristics are strongly dependent on atomic volume, an external pressure, decreasing interionic distances, must strongly affect the values of the exchange integrals.

Consider the experimental data on the pressure and temperature dependence of specific magnetization σ in some amorphous RE – Fe (R – Fe) alloys (Fig. 14). An increase in the magnetization of alloys on cooling is due to the phase transition to an ordered magnetic state at the Curie temperature Θ. The Curie temperature was determined by the thermodynamic-coefficient method [90]. When applying pressure, the $\sigma(T)$ curves shift to lower temperatures, and this effect is maximal for the $Y_{19}Fe_{81}$ alloy. Some relevant parameters for a number of R – Fe alloys are listed in Table 1. Presented here are the Curie temperature Θ determined by the thermodynamic method [90], the Curie temperature shift $\partial\Theta/\partial P$ under the action of pressure, and the parameter Γ, which specifies the relative change of Θ versus

Table 1. Curie temperatures Θ, Curie temperature shifts $\partial\Theta/\partial P$ under pressure and values of the Γ parameter in some amorphous R – Fe alloys.

Composition	Θ, K	$\partial\Theta/\partial P \times 10^9$, K cm^2 dyn^{-1}	Γ
$Y_{19}Fe_{81}$	166	−5.7	46
$Er_{26}Fe_{74}$	212	−3.5	24
$Er_{32}Fe_{68}$	129	−0.85	9
$Er_{54}Fe_{46}$	118	−0.4	4
$Ho_{21}Fe_{79}$	226	−1.64	10
$Dy_{25}Fe_{75}$	267	−2.5	13
$Dy_{59}Fe_{41}$	160	−0.6	4
$Tb_{60}Fe_{40}$	105	−0.5	6

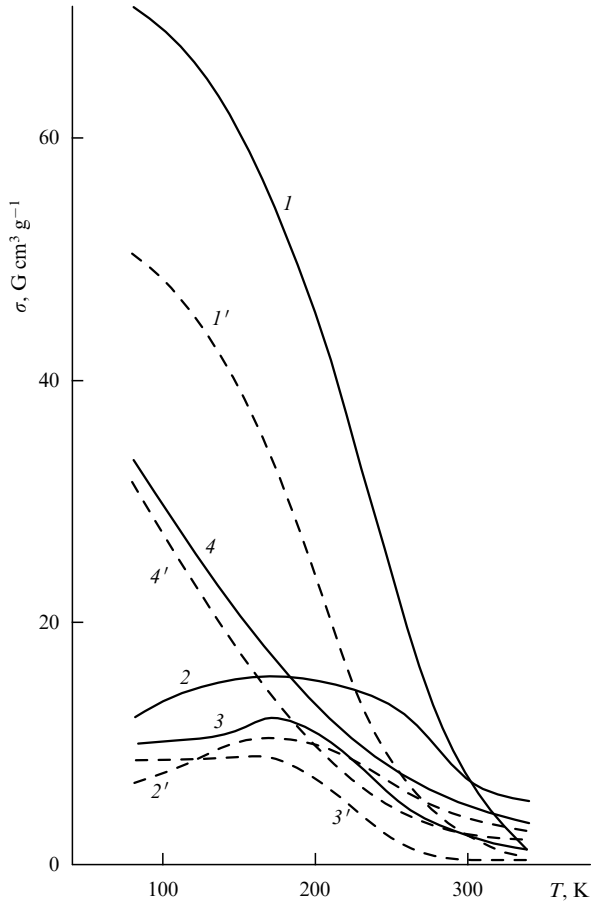

Figure 14. Temperature dependence of the specific magnetization at atmospheric pressure (solid lines) and at a pressure of 10^{10} dyn cm^{-2} (dashed lines) in field $H = 12$ kOe for the amorphous alloys: $Y_{19}Fe_{82}$ (curves *1*, *1′*), $Dy_{25}Fe_{75}$ (*2*, *2′*), $Er_{26}Fe_{74}$ (*3*, *3′*), $Ho_{21}Fe_{79}$ (*4*, *4′*).

the relative change of atomic volume

$$\Gamma = -\frac{1}{\alpha\Theta}\frac{\partial\Theta}{\partial P}\,, \tag{14}$$

where α is the compressibility.

It is known that the magnetic moment of rare-earth ions is strongly localized because of screening of the magnetic 4f electrons by the outer $5s^25p^6$ electron shells. Measurements of hyperfine fields at the ^{57}Fe nuclei [91, 92] showed that the greater part of the 3d electrons in crystalline R – Fe compounds is localized at the iron atoms. In an amorphous state the degree of localization is even further increased because of the decrease in the mean free path of electrons as a result of their scattering on a disordered atomic structure [93]. Strong localization of the 3d electrons at the Fe ions, on the one hand, and the 4f electrons on the RE ions, on the other, allows one to use the molecular-field theory for describing these two magnetic subsystems coupled with each other by the exchange interaction.

In the molecular-field approximation, the Curie temperature Θ for a two-sublattice R – Fe ferrimagnet can be written in the form [94]

$$\Theta = \frac{\Theta_0}{2} + A_2G + \left[\left(\frac{\Theta_0}{2} - A_2G\right)^2 + A_1Gh_{21}^2\right]^{1/2}, \tag{15}$$

where Θ_0 is the Curie temperature of an alloy at which the magnetic moment of the R subsystem is equal to zero; G is the de Gennes factor for the RE ion, h_{21} is the molecular-field constant which determines the value of the effective molecular field acting on the R subsystem from the Fe subsystem

$$h_{21} = \frac{z_{21}A_{21}s_1}{\mu_B} \tag{16}$$

(s_1 is the spin of the Fe ion, A_{21} is the effective R – Fe exchange integral, and z_{21} is the number of nearest neighbors of the RE ion in the Fe subsystem);

$$A_1 = \frac{4\mu_B^2}{9k_B^2}\frac{v_2}{v_1}\frac{s_1+1}{s_1}\,, \tag{17}$$

where v_1 and v_2 are the numbers of the Fe and RE ions per molecular unit, respectively; k_B is the Boltzmann constant; and μ_B is the Bohr magneton.

Upon proper manipulation, Eqn (15) can be reduced to the form

$$\Theta\frac{\Delta\Theta}{G} = A_1h_{21}^2 + 2A_2\Delta\Theta\,. \tag{18}$$

Here the coefficient A_2 is determined by the formula

$$A_2 = z_{22}\frac{A_{22}}{3k_B}\,,$$

where A_{22} is the R – R exchange integral, and z_{22} is the number of nearest neighbors of the RE ion in the R subsystem.

In view of weakness of the f – f exchange, the second term in Eqn (18) can be neglected.

It follows from Eqn (18) that a linear relationship between the quantity $\Theta\Delta\Theta$ and the de Gennes factor must be held. Figure 15 illustrates the $\Theta\Delta\Theta(G)$ dependence for the averaged composition $R_{22}Fe_{78}$. As is seen from this figure, this dependence is linear, which correlates well with the concept of a localized magnetic moment of Fe ions and testifies to the retention of properties of the Fe subsystem upon varying composition. The value of the molecular field acting on the R subsystem was calculated from the slope of the corresponding straight line [87, 89]; this value has been found to be $h_{21} = 1.7 \times 10^6$ Oe. Hence, in view of Eqn (16), the exchange integral is equal to $A_{21} = 1.3 \times 10^{-15}$ erg $= 9.4$ K. It should be noted that in the crystalline RFe_3 compounds closest in composition to amorphous alloys under discussion, the molecular field h_{21} is 5.7×10^6 Oe [94].

The molecular field coefficient h_{11} for the exchange interaction within the Fe subsystem was determined from the Curie temperature of the $Y_{19}Fe_{81}$ alloy using the following formula [94]:

$$h_{11} = \frac{3k_B\Theta_0}{2\mu_B(s+1)}\,. \tag{19}$$

In the absence of magnetic RE ions, the molecular field h_{11} in the Fe subsystem of the amorphous $R_{22}Fe_{78}$ alloys is 1.9×10^6 Oe. This corresponds to a value of $A_{11} = 2.9 \times 10^{-15}$ erg $= 20.8$ K for the Fe – Fe exchange integral. Since in the crystalline RFe_3 compounds $h_{11} = 8 \times 10^6$ Oe [93], the values of the Fe – Fe exchange fields in amorphous R – Fe alloys are less than those in crystalline compounds with analogous compositions.

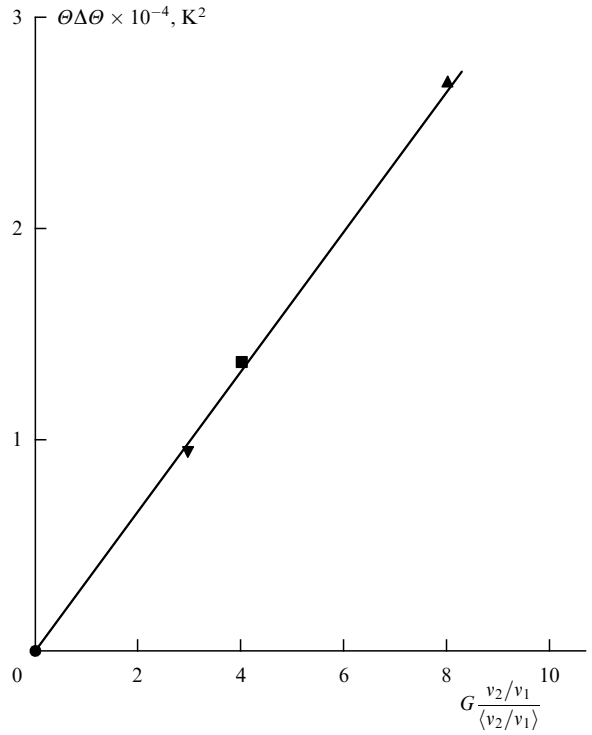

Figure 15. Dependence of $\Theta\Delta\Theta$ on the de Gennes factor G for amorphous alloys of the effective composition $R_{22}Fe_{78}$.

Using the molecular field theory, the atomic-volume dependence of the exchange integrals A_{11} and A_{21} was calculated. Differentiating Eqn (19) with respect to pressure and taking into account the relation

$$h_{11} = \frac{z_{11} A_{11} s_1}{\mu_B}$$

and Hooke's law for a relative change of volume $\Delta V/V$ under pressure ΔP in the form $\Delta V/V = \Delta P/\alpha$, we obtain

$$\frac{\partial A_{11}}{\partial \ln V} = -\frac{1}{\alpha} \frac{3k_B}{2s_1(s_1+1)z_{11}} \frac{\partial \Theta_0}{\partial P} . \tag{20}$$

Differentiating Eqn (18), neglecting the small second term in this equation, and using formula (16), we obtain

$$\frac{\partial |A_{21}|}{\partial \ln V} = -\frac{1}{\alpha} \frac{\mu_B}{s_1 z_{21}} \left[\Delta\Theta \frac{\partial \Theta}{\partial P} + \Theta\left(\frac{\partial \Theta}{\partial P} - \frac{\partial \Theta_0}{\partial P}\right)\right] \frac{1}{2|h_{21}| G A_1} . \tag{21}$$

The calculation results are presented in Table 2.

It is seen from the data given in Table 2 that A_{11} and A_{21} decrease with increasing atomic volume. However, because these integrals are opposite in sign ($A_{11} > 0$ and $A_{21} < 0$), the absolute value of A_{11} decreases, whereas that of A_{21} increases.

Table 2. Exchange integrals and their derivatives with respect to atomic volume for amorphous alloys of the average composition $R_{22}Fe_{78}$.

Composition	A_{11}, K	A_{21}, K	$\frac{\partial A_{11}}{\partial \ln V}$, K	$\frac{\partial \lvert A_{21}\rvert}{\partial \ln V}$, K	$\frac{\partial \ln A_{11}}{\partial \ln V}$	$\frac{\partial \ln \lvert A_{21}\rvert}{\partial \ln V}$
$Er_{26}Fe_{74}$	20.8	−9.4	950	−187	46	−20
$Ho_{21}Fe_{79}$	20.8	−9.4	950	−403	46	−49
$Dy_{25}Fe_{75}$	20.8	−9.4	950	−134	46	−14
$Y_{19}Fe_{81}$	20.8	—	950	—	46	—

Let us consider the reason for the increase of $|A_{21}|$ as the atomic volume decreases. The R – Fe interaction was shown to be covalent in character and arise from hybridization of the 3d electrons of iron with the 5d electrons of the rare-earth element [95 – 98]. As this hybridization takes place, in the vicinity of the RE ion a local magnetic moment of the 5d electrons is formed. Such a moment is opposite in direction to the magnetic moment of iron and interacts with the 4f electrons of the RE ion through the intra-atomic f – d exchange. The intra-atomic 4f – 5d interaction is positive, so that the spin of the 4f ion eventually turns to be directed opposite to the spin of the 3d electrons of the transition metal. Theoretical estimate shows that in the XFe_2 compounds (X = Y, Lu, Zr) the magnetic moment of the X ion, which has no localized magnetic moment, range from 0.33 to 0.43 μ_B [96 – 99]. Experimental investigations of hyperfine fields [97, 100, 101] and the effect of pressure on magnetization in the Y – Fe and Zr – Fe [102] compounds indirectly confirm the theoretical estimates.

A decrease in the interatomic distances under the action of pressure results in an increase of the degree of hybridization of the 3d and 5d electrons. This, in turn, causes the localized magnetic moment of the 5d electrons and the value of the effective exchange integral A_{21} to increase, which is in agreement with experimental results (Table 2).

The mechanisms of exchange interactions within the transition metal subsystem in intermetallic compounds were considered in Ref. [103]. It was shown that the 3d – 3d exchange interaction may be described in terms of two contributions: (1) the direct 3d – 3d exchange and (2) the indirect 3d – 5d – 3d exchange as a result of the 5d – 3d hybridization. The latter contribution allows one to attribute the distinctions in the Curie temperatures for isostructural Y – 3d and (La, Lu) – 3d compounds to the difference in the values of the 4d – 5d and 5d – 3d interaction energies.

The data presented in Table 2 suggest that the ferromagnetic interactions within the Fe subsystem weaken when applying pressure ($\partial A_{11}/\partial \ln V = 950 > 0$). Based on the theoretical papers mentioned above, one can attribute this fact to the strengthening of the overlap and hybridization of the d electron wave functions with decreasing interatomic distances.

It follows from Table 2 that the derivatives $\partial A_{11}/\partial \ln V$ and $\partial |A_{21}|/\partial \ln V$ are opposite in sign. Hence, changes of exchange interactions within the Fe subsystem and between the R and Fe subsystems induced by pressure affect the Curie temperature in the opposite manner. This offers an explanation for why the values of the derivative $\partial\Theta/\partial P$ and the parameter Γ decrease with increasing rare-earth content in an alloy (see Table 1) .

According to literature data [94, 104], the derivative $\partial\Theta/\partial P$ in crystalline R – Fe compounds varies not only in magnitude, but also in sign. It is of interest to compare the atomic-volume dependence of exchange integrals in crystalline compounds, on the one hand, and in amorphous alloys, on the other. Based on the data from Refs [94, 104], we calculated the values of $\partial A_{11}/\partial \ln V$ and $\partial |A_{21}|/\partial \ln V$ in the crystalline compounds YFe_3 and $ErFe_3$ (Table 3). A comparison of Tables 2 and 3 shows that the behavior of amorphous alloys differs essentially from that of crystalline compounds: in the crystalline state, the derivative $\partial A_{11}/\partial \ln V$ is close to 0, whereas in the amorphous state it is rather large ($\simeq$ 950 K).

Table 3. Exchange integrals and their derivatives with respect to atomic volume for the crystalline intermetallic compounds RFe_3.

Composition	A_{11}, K	A_{21}, K	$\frac{\partial A_{11}}{\partial \ln V}$, K	$\frac{\partial \lvert A_{21}\rvert}{\partial \ln V}$, K	$\frac{\partial \ln A_{11}}{\partial \ln V}$	$\frac{\partial \ln \lvert A_{21}\rvert}{\partial \ln V}$
YFe_3	154	—	0	—	0	—
$ErFe_3$	154	−51	0	23	0	0.5

The derivatives $\partial|A_{21}|/\partial \ln V$ are opposite in sign in these two states. This distinction is likely attributable to the difference in the local environment of magnetic ions in amorphous and crystalline compounds.

Thus, the experimental data for the effects of pressure on the Curie temperature of amorphous R – Fe alloys and the molecular field calculations show that the positive (ferromagnetic) Fe – Fe exchange interaction decreases and the negative (antiferromagnetic) R – Fe exchange interaction increases (in absolute value) with increasing pressure. The latter fact may be explained by increasing of the 3d – 5d hybridization with decreasing interatomic distances.

4.2 Effect of pressure on the magnetic structures of amorphous R – Fe alloys

Exchange interactions in the Fe subsystem of amorphous and crystalline R – Fe alloys are of fundamental importance in determining their magnetic structures. To eliminate from consideration exchange interactions between sublattices and exchange interactions within the rare-earth subsystem, the substitution of trivalent magnetic RE ions by yttrium, which is also trivalent, is frequently used. Yttrium is a Pauli paramagnet, has a metallic radius (1.80 A) close to that of RE ions (1.75 – 1.83 A), and is an ideal 'dilutant' for amorphous alloys and crystalline rare-earth compounds.

At low temperatures in the amorphous Y_xFe_{100-x} alloys with a high content of iron ($x < 57$), a reentrant spin-glass state [105 – 107] and invar properties [86, 108] are found experimentally. The magnetic moment of iron μ strongly depends on concentration and compositional short-range order: a noticeable moment appears at $x < 60$, when more than six Fe ions are present among the nearest neighbors of a given Fe ion [105, 106, 109, 110]. At concentrations $20 < x < 60$, magnetic and nonmagnetic Fe ions coexist.

As was shown above, the exchange interactions within the Fe subsystem are strongly dependent on the distance between the Fe ions. Therefore, an external pressure would be expected to affect not only the temperatures, but also the character of magnetic phase transitions [86, 89].

Figure 16 shows the temperature dependence of ZFC magnetization for the amorphous $Y_{19}Fe_{81}$ alloy measured during the warming-up of a sample in various magnetic fields and the temperature dependence of the initial susceptibility $\chi(T)$. The Curie temperature determined by the thermodynamic-coefficient method [90] was found to be 166 K. Temperature hysteresis at low temperatures, upon both ZFC and FC, indicates that the alloy changes to a reentrant spin-glass state at these temperatures. The shape of the $\chi(T)$ curve shows that a sharp decrease in susceptibility at $T_f = 120$ K is also due to this transition. The same $\chi(T)$ dependence was observed close to T_f in other amorphous alloys changing to a reentrant spin-glass state [111, 112].

The $\chi(T)$ curve substantially changes under the action of pressure (Fig. 17). A plateau observed at atmospheric pressure in the temperature range Θ to T_f corresponding to the region of magnetic ordering narrows and shifts to low

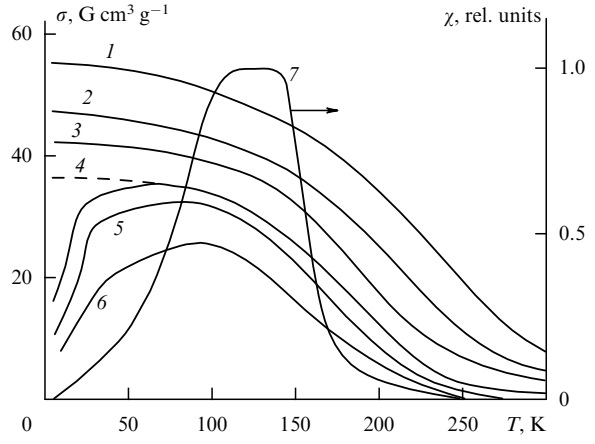

Figure 16. Temperature dependences $\sigma(T)$ and $\chi(T)$ for the amorphous $Y_{19}Fe_{81}$ alloy at atmospheric pressure. Solid lines correspond to the ZFC mode, dashed line, to the FC mode. Curve *1* is measured in magnetic field $H = 14$ kOe, (*2*) 2 kOe, (*3*) 3 kOe, (*4*) 1 kOe, (*5*) 0.5 kOe, and (*6*) 0.12 kOe. Curve *7* stands for $\chi(T)$.

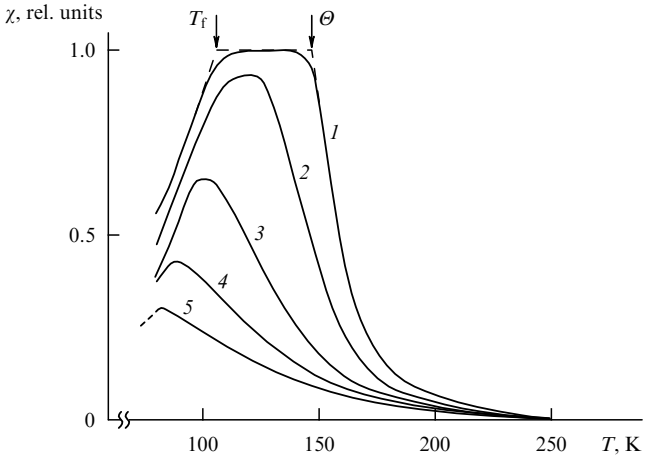

Figure 17. Temperature dependence of the magnetic susceptibility for the amorphous $Y_{19}Fe_{81}$ alloy at different pressures: *1*, atmospheric pressure; (*2*) 3.3; (*3*) 4.9; (*4*) 6.4; and (*5*) 8×10^9 dyn cm^{-2}.

temperatures with increasing pressure. When the pressure exceeds $P = 5.7 \times 10^9$ dyn cm^{-2}, this plateau changes into a maximum. The latter is attributable to the direct transition 'paramagnetic phase-spin-glass state' at temperature Θ_f ($\Theta_f = 93$ K at pressure $P = 5.7 \times 10^9$ dyn cm^{-2}). A similar transformation of the $\chi(T)$ curves under the action of pressure was also observed in the amorphous alloy $La_{12.5}Fe_{87.5}$ [113].

The transition to a spin-glass-like state in amorphous Y – Fe alloys at low temperatures is attributable to the fact that in disordered systems the Fe – Fe exchange interaction varies randomly not only in magnitude, but also in sign. The relative increase of the negative contribution in the Fe – Fe exchange interaction under the action of pressure will result in a considerable shift of the Curie temperature toward low temperatures and only slightly affect the temperature of the transition to a spin-glass-like state. It follows from the $T-P$ phase diagram presented in Ref. [114] that an increase of the atomic volume leads to the destruction of ferromagnetic ordering in the Fe subsystem, with the result that two phase

transitions ('paramagnetic – ferromagnetic' and 'ferromagnetic – reentrant spin glass') transform into one phase transition ('paramagnetic – spin glass').

The investigation of the effect of pressure on phase transitions in the alloys $Dy_{25}Fe_{75}$ and $Er_{24}Fe_{76}$ and in a number of R_xFe_{100-x} alloys with $x > 30$ at.% was also carried out in Ref. [114].

When considering the effect of pressure on phase transitions in R – Fe alloys, two further points must be taken into account. First, the antiferromagnetic interactions between the R and Fe subsystems must be added to the exchange interaction within the Fe subsystem. Second, the ionic radii of rare-earth metals are smaller than the ionic radius of yttrium, with the result that the distance between the Fe ions becomes smaller than in Y – Fe alloys and the negative exchange interactions in the Fe subsystem are enhanced on the account of overlapping of the wave functions of the 3d electrons.

It is of interest to compare the effect of pressure on the magnetic structures of amorphous alloys, on the one hand, and of crystalline compounds, on the other. As was shown in Ref. [115], in the crystalline compounds R_2Fe_{17} an external pressure also causes a magnetic structure to transform, resulting in non-collinear ordering.

Thus, both in amorphous alloys and in crystalline R – Fe compounds a decrease of interatomic distances results in strengthening of antiferromagnetic interactions in the Fe subsystem. Analogous results were obtained for amorphous R – Co alloys [116].

4.3 Effect of pressure on magnetization

The change of magnetization under the action of pressure ($\Delta\sigma$ effect) carries important information about the dependence of exchange integrals and local magnetic anisotropy on atomic volume. Literature data on the investigations of the $\Delta\sigma$ effect in amorphous alloys are scarce. The results of the $\Delta\sigma$-effect measurements depending on temperature and magnetic field, as well as the calculations of the relative $\Delta\sigma$ effect for a number of amorphous alloys, can be found in Refs [87, 88].

To estimate the $\Delta\sigma$ effect in amorphous alloys, the magnetization curves $\sigma(H)$ were measured at atmospheric pressure and at pressure $P = 10^{10}$ dyn cm^{-2}. The temperature and pressure dependences of $\partial\sigma/\partial P$ were calculated from these experimental curves.

The temperature dependences of $\partial\sigma/\partial P$ for the amorphous alloys $Y_{19}Fe_{81}$ and $Er_{26}Fe_{74}$ are shown in Fig. 18. As is seen from this figure, the maximum on the $\partial\sigma/\partial P$ curves in the vicinity of the Curie temperature moves toward higher temperatures as the field increases.

The $\partial\sigma/\partial P$ curves and the $\sigma(H)$ isotherms were used in calculations of the field dependence of the relative $\Delta\sigma$ effect $(\sigma^{-1}\partial\sigma/\partial P)$ in amorphous R – Fe alloys at fixed temperatures $T < \Theta$. It is seen from Fig. 19 that near the Curie temperature and below, two straight segments can be distinguished in the curves of the field dependences of the relative $\Delta\sigma$ effect: one in the low-field region and the other in the high-field region. The bending point, which demarcates these two portions of the curve, lies in the range of 2 – 7 kOe, depending on temperature. At temperatures below Θ, the quantity $\sigma^{-1}\partial\sigma/\partial P$ markedly changes with magnetic field in the first region and is nearly constant in the second region.

The results presented above testify the existence of two different mechanisms of magnetization processes. To discuss these results, we note the formula describing the

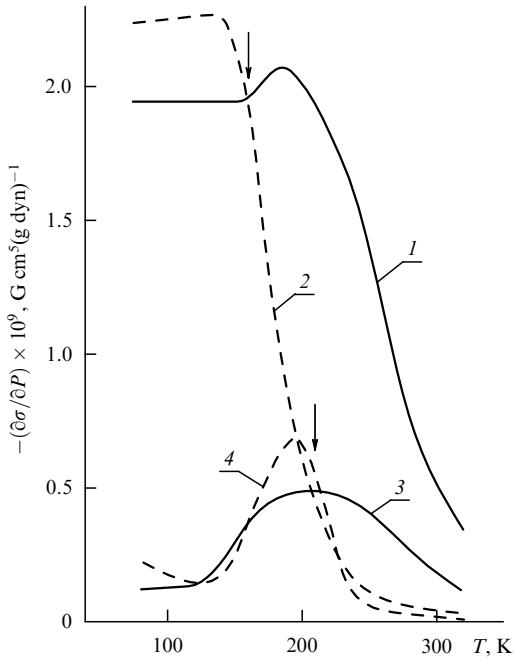

Figure 18. Temperature dependences of the $\Delta\sigma$ effect for the amorphous alloys $Y_{19}Fe_{81}$ [(*1*) $H = 12$ kOe, (*2*) $H = 1$ kOe] and $Er_{26}Fe_{74}$ [(*3*) $H = 12$ kOe, (*4*) $H = 1$ kOe]. Arrows point the Curie temperatures.

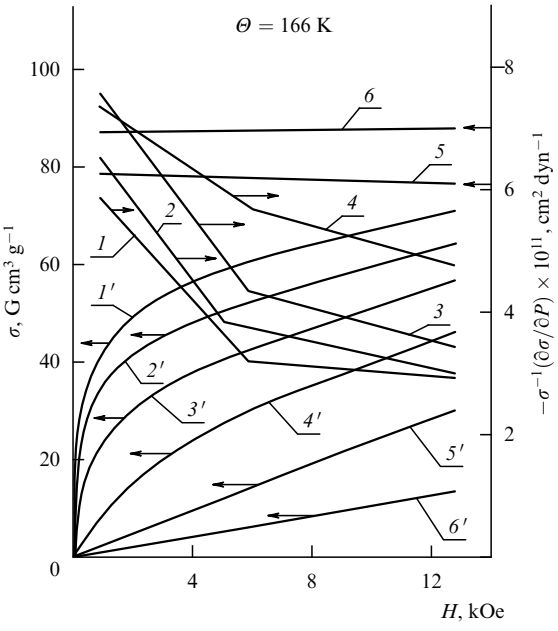

Figure 19. Field dependences of the relative $\Delta\sigma$ effect (curves *1* – *6*) and specific magnetization σ (curves *1′* – *6′*) for the amorphous $Y_{19}Fe_{81}$ alloy at different temperatures: (*1*, *1′*) 80 K, (*2*, *2′*) 130 K, (*3*, *3′*) 165 K, (*4*, *4′*) 200 K, (*5*, *5′*) 240 K, and (*6*, *6′*) 280 K.

$\Delta\sigma$ effect [117]

$$\frac{1}{\sigma_s}\frac{\partial\sigma_s}{\partial P} = \frac{1}{\sigma_s}\frac{\partial\sigma_0}{\partial P} - \frac{1}{\sigma_s}\frac{\partial\sigma_s}{\partial T}\frac{T}{P}\frac{\partial\Theta}{\partial P}, \qquad (22)$$

where σ_0 is the specific saturation magnetization at $T = 0$ K, and σ_s is the specific spontaneous magnetization at an arbitrary temperature.

Here, the first term is a contribution to the $\Delta\sigma$ effect from the change in the saturation magnetization at $T = 0$ under the action of pressure. The second term describes the Curie-temperature shift with pressure and, hence, determines the contribution associated with the pressure change of exchange interaction.

In high magnetic fields and at low temperatures $T \ll \Theta$, when the magnetization process is virtually completed, the $\Delta\sigma$ effect varies only slightly, so that by analogy with the foregoing equation one can write

$$\frac{1}{\sigma}\frac{\partial\sigma}{\partial P} = \frac{1}{\sigma_0}\frac{\partial\sigma_0}{\partial P} - \frac{1}{\sigma}\frac{\partial\sigma}{\partial T}\frac{T}{\Theta}\frac{\partial\Theta}{\partial P}, \qquad (23)$$

where σ is the magnetization in magnetic field H at temperature T and pressure P.

Since pressure does not virtually affect the domain wall displacement [118], one can distinguish two contributions in the magnetization processes in amorphous R – Fe alloys: (1) due to the rotation of the magnetic moments of ions within domains and (2) due to the rotation of the magnetic moments of domains toward the magnetic field direction. According to literature data [15], amorphous rare-earth alloys do not become saturated up to fields of about 200 kOe because of a competition of exchange interactions and random magnetic anisotropy. Thus, the bends in the relative $\Delta\sigma$-effect curves are likely due to the fact that in low fields the magnetization process occurs by rotation of the magnetic moments of domains, and the pressure stimulates this process [the first term in Eqn (23)], whereas in high fields the magnetization increases on the account of rotation of the magnetic moments of individual atoms, and the external pressure, affecting the exchange integrals, enhances this process [the second term in Eqn (23)].

As was shown above, at temperatures < 100 K the amorphous $Y_{19}Fe_{81}$ alloy transforms to a reentrant spin-glass state. It can be assumed that the variation of the relative $\Delta\sigma$ effect in high fields is determined predominantly by the action of pressure on the asperomagnetic cone of iron spins with the resulting increase of average magnetic moment per iron atom.

In the amorphous alloys $Er_{26}Fe_{74}$, $Ho_{21}Fe_{79}$ and $Dy_{25}Fe_{75}$, the magnetic moment also changes under the action of pressure because of increasing degree of noncollinearity in the Fe subsystem.

5. Conclusions

Amorphous rare-earth alloys are so specific with respect to exchange, magnetoanisotropic and magnetoelastic interactions that they may be considered a new class of magnetically ordered substances. Because of the absence of a crystal periodicity, the electron density distribution of the delocalized electrons in the interatomic space of amorphous materials is more localized ('compressed') as a consequence of scattering of these electrons on the disordered atomic structure. In RE – Fe compounds, where the 3d electrons of the iron atoms and the 4f electrons are either essentially (3d) or totally (4f) localized near the atomic cores, this transformation of electron density distribution upon amorphization results in a lowering of the Curie temperature in amorphous alloys relative to that in their crystalline analogs (for example, $\Theta = 388$ K in the amorphous $TbFe_2$ alloy, whereas in its crystalline analog, $\Theta = 710$ K). A dominant role in the lowering of the Curie temperature in an amorphous state is played by the effect of scattering of the 3d and 4f electrons, implementing exchange interaction within a disordered atomic structure.

In RE – Co compounds, on the contrary, the Curie temperature of amorphous alloys is considerably higher than that of their crystalline analogs (for example, $\Theta = 370$ K in the amorphous $TbCo_2$ alloy, whereas in its crystalline analog, $\Theta = 256$ K). Here, the magnetism of the Co sublattice is itinerant in character: the 3d electrons are smeared over space and their magnetic moment is determined by the difference in the degree of occupation of 'spin-up' and 'spin-down' 3d subbands. Scattering of the 3d electrons on a disordered atomic structure appears to increase their localization in the vicinity of atomic cores, increasing the 3d subband shift on the account of exchange interaction and an increase of the Curie temperature in amorphous alloys as compared to their crystalline analogs. The experimental data on the Curie-temperature shift under the action of pressure shows that the atomic-volume dependence of exchange integrals in amorphous alloys differs essentially from that in crystalline compounds. This testifies to a considerable difference in the overlap of the wave functions of not only 3d, but also 5d electrons involved in exchange interaction.

Other features of amorphous alloys are associated with the fact that magnetic anisotropy manifests itself in them mainly as local anisotropy in the vicinity of atomic cores. Because of its combination with induced anisotropy as well as the presence of stiff domain walls, magnetization processes take on properties entirely different from those of the classic ferromagnets. Among these are the formation of a spin 'fan' as the magnetization rotates, the appearance of 'forbidden' spin orientations, breaking of the standard sequence of magnetization processes (with rotation occurring before displacement), etc.

The existence of microscopic nanometer-sized regions and the possibility of creating intermediate states bordering crystal ones (nanostructural states) allow one, in principle, to obtain materials in which magnetization processes proceed in these microscopic regions regardless of the surrounding magnetic matrix. This makes it possible to use amorphous materials as magnetic recording media with ultra-high information-storage densities where these nanometer-sized regions play the role of unit storage cells. At present, RE-materials are only at the very beginning of their active application in technology. Using annealing, fine-grained films with high magnetic energy can be fabricated from magnetic layers [10, 11]. Such film magnets are very promising for microwave technology and magnetic and magnetooptic recording.

The investigation of the propagation of spin and acoustic waves in amorphous alloys [118], magnetoacoustic resonance previously studied in crystalline compounds [119], and some other effects appear to have considerable promise.

There is no question that the theoretical concepts developed for amorphous alloys will find wide utility in studies of other disordered systems such as quasicrystals, fractals, magnetic polymers, etc.

Acknowledgments

The authors are very grateful to I Zolotukhin, A Zvezdin, E Sinitsyn, Yu Kalinin for fruitful discussions of the results given in this review. We also thank all post-graduates and students working in the Laboratory of Amorphous and

Crystalline Alloys of Rare-Earth Metals at the Department of Physics, Moscow State University, whose experimental results were used in the review.

References

1. Gubanov A I *Fiz. Tverd. Tela* (Leningrad) **2** 502 (1960)
2. Chaudhari P, Cuomo J J, Gambino R J *IBM J. Res. Dev.* **17** 66 (1973)
3. Rhyne J J, Pickart S J, Alperin H A *Phys. Rev. Lett.* **29** 1562 (1972)
4. Rhyne J J, Schelleng J H, Koon N C *Phys. Rev. B* **10** 4672 (1974)
5. Pickart S J, Rhyne J J, Alperin H A *Phys. Rev. Lett.* **33** 424 (1974)
6. Heinman N, Lee K, Potter R I *AIP Conf. Proc.* **29** 130 (1976)
7. Handrich K, Kobe S *Amorfe Ferro und Ferrimagnetika* (Berlin: Akad. Verlag, 1980) [Translated into Russian (Moscow: Mir, 1982)]
8. Buler P I *Fiz. Khim. Stekla* **18** (5) 119 (1992)
9. Sudzuki K, Fudzimoro Kh, Khasimoto K *Amorfnye Splavy* (Moscow: Metallurgiya, 1991)
10. Kraposhin V Ts, Linetskiĭ Ya L *Itogi Nauki Tekhniki Ser. Metalloved. Term. Obrab.* (Moscow: VINITI, 1982) Vol. 16 p. 1
11. Salo I P, Thesis for Candidate of Physicomathematical Sciences (Moscow: MISIS, 1985)
12. Manakov N A, Thesis for Doctorate of Physicomathematical Sciences (Irkutsk: IPI, 1994)
13. Zolotukhin I V, Kalinin Yu E *Usp. Fiz. Nauk* **160** (9) 75 (1990) [*Sov. Phys. Usp.* **33** 720 (1990)]
14. Belov K P *Magnitostriktsionnye Yavleniya i Ikh Tekhnicheskie Prilozheniya* (Magnetostriction Phenomena and Their Engineering Applications) (Moscow: Nauka, 1987)
15. Moorjani K, Coey J M D *Magnetic Glasses* (Amsterdam: Elsevier, 1984) p. 450
16. Andreenko A S et al. *Zh. Eksp. Teor. Fiz.* **99** 540 (1991) [*Sov. Phys. JETP* **72** 301 (1991)]
17. Imry Y, Ma S-k *Phys. Rev. Lett.* **35** 1399 (1975)
18. Harris R, Plischke M, Zuckermann M J *Phys. Rev. Lett.* **31** 160 (1973)
19. Andreenko A S, Thesis for Doctorate of Physicomathematical Sciences (Moscow: Moscow State Univ., 1994)
20. Nikitin S A et al. *Fiz. Tverd. Tela* (Leningrad) **29** 1526 (1987) [*Sov. Phys. Solid State* **29** 874 (1987)]
21. Sinitsyn E V et al. *Fiz. Met. Metalloved.* **54** 723 (1982)
22. Sinitsyn E V, Thesis for Doctorate of Physicomathematical Sciences (Sverdlovsk: Ural. Inst. of Mining, 1988)
23. Belov K P et al. *Orientatsionnye Perekhody v Redkozemel'nykh Magnetikakh* (Orientational Transitions in Rare-Earth Magnets) (Moscow: Nauka, 1979)
24. Andreenko A S et al. *Fiz. Tverd. Tela* (Leningrad) **30** 3002 (1988) [*Sov. Phys. Solid State* **30** 1729 (1988)]
25. Kobayashi H et al. *Appl. Phys. Lett.* **43** 389 (1983)
26. Takeno Y et al. *Jpn. J. Appl. Phys.* **25** L657 (1986)
27. Wang Y J et al. *J. Phys.* (Paris) C **40** 239 (1989)
28. Yoshino S et al. *Jpn. J. Appl. Phys.* **23** 188 (1984)
29. Gronan M, Schuffler D, Sprenger S *IEEE Trans. Magn.* **MAG-20** 66 (1984)
30. Sakurai Y, Onishi K *J. Magn. Magn. Mater.* **35** 183 (1983)
31. Shimanuki S et al. *IEEE Trans. J. Magn. Jpn.* **TJMJ-2** 338 (1987)
32. Suzuki Y et al. *IEEE Trans. Magn.* **MAG-23** 2275 (1987)
33. Mimura Y et al. *J. Appl. Phys.* **49** 1208 (1978)
34. Lee Zo-Yi, Numata T, Sakurai Y *Jpn. J. Appl. Phys.* **22** L600 (1983)
35. Okamine S, Ohta N, Sugita Y *IEEE Trans. Magn.* **MAG-21** 1641 (1985)
36. Mimura Y, Imamura N *Appl. Phys. Lett.* **28** 746 (1976)
37. Gronan M, Goeke H, Methfessel S, in *Proc. 4th Int. Conf. on Rapidly Quenched Metals* (1981) p. 897
38. Lee Z Y et al. *IEEE Trans. Magn.* **MAG-20** 1335 (1984)
39. Suran G, Ounadjela K *J. Magn. Magn. Mater.* **54 – 57** 237 (1986)
40. Suran G, Naili M, Sztern J *J. Appl. Phys.* **63** 4318 (1988)
41. Egami T et al. *IEEE Trans. Magn.* **MAG-23** 2269 (1987)
42. Glazer A A, Tagirov R I *Izv. Akad. Nauk SSSR Ser. Fiz.* **42** 1600 (1978) [*Bull. Acad. Sci. USSR Ser. Phys.* **42** 27 (1978)]
43. Nikitin S A, Andreenko A S, Damianova R N *IEEE Trans. Magn.* **3** 1987 (1988)
44. Zolotukhin I V *Fizicheskie Svoĭstva Amorfnykh Metallicheskikh Materialov* (Physical Properties of Amorphous Metallic Materials) (Moscow: Metallurgiya,1986) p. 176
45. Damianova R et al. *J. Magn. Magn. Mater.* **123** 325 (1993)
46. Andreenko A S et al. *Fiz. Tverd. Tela* (Leningrad) **32** 1020 (1990)
47. Andreenko A S, Damyanova R N, Yakovlev V I *Fiz. Tverd. Tela* (Leningrad) **35** 2432 (1993)
48. Nikitin S A *Magnitnye Svoĭstva Redkozemel'nykh Metallov i Ikh Splavov* (Magnetic Properties of Rare-Earth Metals and Their Alloys) (Moscow: Moscow State Univ. Press,1989)
49. Fujiwara H et al. *J. Phys. Soc. Jpn.* **42** 1194 (1977)
50. Bartholin H, Bloch D *J. Phys. Chem. Solids* **29** 1063 (1968)
51. McWhan D B, Stevens A L *Phys. Rev.* **154** 438 (1967)
52. McWhan D B, Stevens A L *Phys. Rev.* **139** 682 (1965)
53. Vinokurova L I et al. *Fiz. Tverd. Tela* (Leningrad) **14** 720 (1972) [*Sov. Phys. Solid State* **14** 613 (1972)]
54. Nikitin S A, Bezdushnyĭ R V *Fiz. Tverd. Tela* (Leningrad) **31** 306 (1989)
55. Nikitin S A, Leont'ev P I *Fiz. Tverd. Tela* (Leningrad) **29** 2147 (1987) [*Sov. Phys. Solid State* **29** 1235 (1987)]
56. Nikitin S A, Leont'ev P I *Fiz. Met. Metalloved.* **64** 81 (1987)
57. Nikitin S A, Besduschni R V *Phys. Status Solidi A* **124** 327 (1991)
58. Robinson L B, Tan S-I, Sterrett K F *Phys. Rev.* **141** 548 (1966)
59. Milton J E, Scott T A *Phys. Rev.* **160** 387 (1967)
60. Lindgren B, Mayer A *J. Magn. Magn. Mater.* **84** 115 (1990)
61. Jayaraman A, in *Handbook on the Physics and Chemistry of Rare Earths* Vol. 1 (Eds K A Gschneidner, L R Eyring) (Amsterdam: Elsevier, 1978) p. 707
62. Yang T T, Robinson L B *Phys. Rev.* **185** 743 (1969)
63. Milstein F,Robinson L B *Phys. Rev.* **159** 466 (1967)
64. Achiwa N et al. *J. Phys. Collog.* (France) **49** (C-8) 349 (1988)
65. Wohlfarth E P *J. Phys. C*: *Sol. St. Phys.* **2** 68 (1969)
66. Edwards D M, Wohlfarth E P *Proc. R. Soc. London Ser. A* **303** 127 (1968)
67. Heine V *Phys. Rev.* **153** 673 (1967)
68. Lang N D, Ehrenreich H *Phys. Rev.* **168** 605 (1968)
69. Shiga M *Solid State Commun.* **7** 559 (1969)
70. Shimizu M *Rep. Prog. Phys.* **44** 329 (1981)
71. Takahashi T, Shimizu M *J. Phys. Soc. Jpn.* **20** 26 (1965)
72. Bloch D, Lemaire R *Phys. Rev. B* **2** 2648 (1970)
73. Voiron J et al. *Solid State Commun.* **13** 201 (1973)
74. Inoue J, Shimizu M *J. Phys. F*: *Met. Phys.* **10** 721 (1980)
75. Leont'ev P I et al. *Fiz. Tverd. Tela* (Leningrad) **30** 3700 (1988) [*Sov. Phys. Solid State* **30** 2125 (1988)]
76. Shirakawa K et al. *J. Appl. Phys.* **52** 1829 (1981)
77. Jageilinski T et al. *Solid State Commun.* **44** 225 (1982)
78. Shirakawa K et al. *Sci. Rep. Res. Inst. Tohoku Univ. Ser. A* **31** 54 (1983)
79. Kamarad J, Arnold Z *Physica B+C* **139** 184 (1986)
80. Biesterbos J W M, Broucha M, Dirks A G *AIP Conf. Proc.* **29** 184 (1976)
81. Shirakawa K et al. *J. Phys. F*: *Met. Phys.* **15** 961 (1985)
82. Bielle J, Lienard A, Rebouillat J P *J. Phys. Collog.* (France) **40** 256 (1979)
83. Ishio S *J. Phys. Collog.* (France) **49** 1345 (1988)
84. Ishio S, Yang X, Miyazaki T *J. Phys*: *Condens. Matter* **1** 8979 (1989)
85. Ishio S et al. *J. Phys. F*: *Met. Phys.* **18** 2253 (1988)
86. Andreenko A S et al. *J. Magn. Magn. Mater.* **118** 147 (1993)
87. Andreenko A S, Nikitin S A, Spichkin Yu I *J. Magn. Magn. Mater.* **118** 142 (1993)
88. Andreenko A S, Nikitin S A, Spichkin Yu A *Fiz. Tverd. Tela* (Leningrad) **37** 1643 (1995)
89. Andreenko A S, Nikitin S A, Spichkin Yu A *Vestn. Mosk. Univ. Fiz. Astron.* **34** 55 (1993) [*Mosc. Univ. Phys. Bull.* **48** 48 (1993)]
90. Belov K P *Magnitnye Prevrashcheniya* (Moscow: Fizmatgiz, 1959) [Translated into English *Magnetic Transformations* (New York: Consultants Bureau, 1961)]
91. Nikitin S A et al. *Fiz. Tverd. Tela* (Leningrad) **16** 3137 (1974) [*Sov. Phys. Solid State* **16** 2031 (1975)]
92. Stearns M B *Phys. Rev. B* **8** 4383 (1973)
93. Vedyaev A V, Granovskiĭ A B, Kotel'nikova O A *Kineticheskie Yavleniya v Neuporyadochennykh Ferromagnitnykh Splavakh* (Ki-

netic Phenomena in Disordered Ferromagnetic Alloys) (Moscow: Moscow State Univ., 1992)
94. Nikitin S A, Bisliev A M *Vestn. Mosk. Univ. Fiz. Astron.* **16** (2) 195 (1975)
95. Brouha M, Buschow K H J, Miedema A R *IEEE Trans. Magn.* **MAG-10** 182 (1974)
96. Chou C P, Davis L A, Narasimhan M C *Scr. Metall.* **11** 417 (1977)
97. Vasil'kovskiĭ V A et al. *Zh. Eksp. Teor. Fiz.* **97** 1041 (1990) [*Sov. Phys. JETP* **70** 584 (1990)]
98. Mohn P, Schwarz K *Physica B + C* **130** 26 (1985)
99. Jamada H *Physica B* **149** 390 (1988)
100. Brooks M S S, Eriksson O, Johansson B *J. Phys.: Condens. Matter* **1** 5861 (1989)
101. Armitage J G M et al. *J. Phys.: Condens. Matter* **1** 3987 (1989)
102. Dumelow T et al. *J. Magn. Magn. Mater.* **54 – 57** 1081 (1986)
103. Shimizu K *J. Magn. Magn. Mater.* **70** 178 (1987)
104. Brouha M, Buschow K H J *J. Appl. Phys.* **44** 1813 (1973)
105. Chappert J et al. *J. Phys. F* **11** 2727 (1981)
106. Coey J M D et al. *J. Phys. F: Met. Phys.* **11** 2707 (1981)
107. Biesterbos J W M, Brouha M, Dirks A G *Physica B* **86 – 88** 770 (1977)
108. Ishio S et al. *J. Magn. Magn. Mater.* **60** 236 (1986)
109. Chappert J, Arrese-Boggiano R *J. Magn. Magn. Mater.* **7** 175 (1978)
110. Van der Kraan A M, Buschow K H J *Phys. Rev. B* **25** 3311 (1982)
111. Wakabayashi H et al., in *Proc. Int. Symp. Phys. Magn. Mater.* (*ISPMM-87*) (Sendai, 1987) p. 342
112. Skumryev V et al. *J. Phys. Collog.* (France) **49** (C-8) 1363 (1988)
113. Goto T et al. *J. Phys. Collog.* (France) **49** (C-8) 1143 (1988)
114. Andreenko A S, Nikitin S A, Spichkin Yu I *Fiz. Tverd. Tela* **36** 3481 (1994)
115. Andreenko A S, Nikitin S A, Spichkin Yu I *Fiz. Tverd. Tela* **34** 1823 (1992) [*Sov. Phys. Solid State* **34** 1386 (1992)]
116. Bezduschny R et al. *J. Magn. Magn. Mater.* **124** 330 (1993)
117. Bloch D, Drs. Sciences Physiques (Paris, 1965)
118. Andreenko A S, Solodov I Yu, in *Proc. Smart Struct. Mater., SPIE* **2722** 266 (1996)
119. Belyaeva O Yu, Zarembo L K, Karpachev S N *Usp. Fiz. Nauk* **162** 107 (1992) [*Sov. Phys. Usp.* **35** 106 (1992)]